Mathematical Biosciences and Engineering

https://www.aimspress.com/journal/mbe

MBE, 22(12): 3154–3200.
DOI: 10.3934/mbe.2025117
Received: 04 May 2025
Revised: 22 August 2025
Accepted: 17 September 2025
Published: 03 November 2025

Research article

A detailed analysis of the spatial dynamics of a food-chain model with Allee and fear effect

Swati Mishra[1,2], Anal Chatterjee[3,*], Ranjit Kumar Upadhyay[4] and Mainul Haque[5]

[1] Delhi School of Climate Change & Sustainability, Institution of Eminence, University of Delhi, Delhi 110007, India

[2] Faculty of Mathematical Sciences, South Asian University, New Delhi 110068, India

[3] Department of Mathematics, Barrackpore Rastraguru Surendranath College, Kolkata, India

[4] Department of Mathematics & computing, Indian Institute of Technology (Indian School of Mines), Dhanbad 826004, India

[5] School of Mathematical Sciences, University of Nottingham Ningbo China, Ningbo, China

* **Correspondence:** Email: chatterjeeanal172@gmail.com.

Abstract: We investigate the spatiotemporal dynamics of a tri-trophic food chain model incorporating a strong Allee effect on the prey and a fear effect on the middle predator. The model's well-posedness is established through the positivity and boundedness of solutions. We derive all equilibria and examine their local stability, revealing saddle-node and transcritical bifurcations under varying parameter conditions. The analysis demonstrates how shifts in the Allee threshold and fear intensity induce bistability, coexistence, or extinction. Numerical simulations highlight diffusion-driven instabilities and complex Turing patterns, including labyrinthine formations and unexpected "leaser slime" structures—resembling those observed in fungi and algae in aquatic systems. These findings reveal the crucial role of behavioral and ecological feedbacks in shaping pattern formation and species persistence.

Keywords: self-diffusion and cross-diffusion; leaser slime type patterns; two-parameter bifurcation; chaos; food-chain; Allee and fear

1. Introduction

Understanding the factors that influence the stability of food chains is crucial for predicting and managing ecosystem's responses to environmental change. Ecological simulation through mathematical modelling has become a central research direction, underpinning advances in

population dynamics, spatial pattern formation, and ecosystem management [1, 2]. Different mathematical models are proposed, based on biological theories and observations. In [3], Tanner provided a mathematical analysis and simulation of the prey-predator model system considering the intrinsic growth rate of each species population. Prey self-limitation and predators' searching time have the most effect on the stability these models exhibit. The Rosenzweig-MacArthur model [4] is a popular ecosystem model. The Holling Type II functional response is used in this model instead of the linear functional response seen in the Lotka-Volterra model. Gakkhar and Naji [5] examined the dynamical behavior and chaos of a three-species realistic food chain model while considering the interaction's reliance on the ratio of predator to prey and Type II functional response. The model displays stable, periodic, and chaotic dynamics in its long-term behavior for values of biologically acceptable parameters. Hsu et al. [6] partially explained the possible success or failure of biological control in certain situations through a mathematical model of the three-trophic level food chain. Pathak et al. [7] discussed the intricate dynamics of a three trophic food chain model with Hassell Varley functional responses. The discussion analyzes how these concepts shed light on some of the characteristics of actual populations observed in the field. In [8], Upadhyay and Naji conducted an analytical and numerical investigation of a three-species food chain model that includes a hybrid type of prey-dependent and predator-dependent functional responses. It was discovered that the system displays a variety of rich complexity traits, including chaotic, periodic, and stable dynamics. Haque et al. [9] examined the effects of intra-specific competition in a tri-trophic food chain model, where self-interaction elucidated for the first time and discusses real-world applications in conjunction with the analysis results. In [10], Pattanayak et al. re-explored a three-nutrient resource-consumer-predator food chain model and, compared with previous relevant studies, analyzed the system from the perspective of basin stability to provide additional and more precise insights. Feng et al. [11] studied a new model as an extension of the Rosenzweig MacArthur three-trophic food chain model in which the super-predator consumes both the predator and the prey. All possible equilibria were found, and their stability or instability concerning all the ecological parameters was investigated. Kuznetsov et al. [12] examined the intricate dynamics of the most popular tri-trophic food chain model. The model first admits a series of pairs of Belyakov bifurcations (codimension-two homoclinic orbits to a critical node). The general bifurcation scenario demonstrates how odd attractors with diverse geometries coexist with stable limit cycles. Lv and Zhao [13] analyzed a three-species food chain model on the basis of ecological theories and numerical simulation. For biologically practical parameters, bifurcation diagrams were obtained. The investigated model displays numerous complicated properties, including chaotic, periodic, and stable dynamics. Kooi et al. [14] investigated the effects of omnivory on the dynamic behavior of a three-species food web in a chemostat. They employed bifurcation analysis to examine the long-term dynamics under varying levels of omnivory. It was discovered that a weak interaction between the omnivore and its prey and a robust interaction with the predator appears to be beneficial. In [15], the authors studied a class of three-level food chain systems. Using the theory of delay differential equations and Hopf bifurcation, they derived the conditions under which the positive equilibrium undergoes a Hopf bifurcation, taking the delay T as the bifurcation parameter. Recently, the authors of [16, 17] investigated predator-prey models incorporating fear effects, refuge, harvesting, and delays, and analyzed how these factors influence the system's stability and lead to various bifurcations, including Bogdanov-Takens and Hopf bifurcations, supported by theoretical and numerical results.

In [18], Gascoigne and Lipcius studied the impact of the Allee effect on ecological models of species invasion and found that it could prevent the establishment of certain species during biological invasions. This indicates that the Allee effect will produce extinction thresholds for populations with sparse species density to a certain extent. The model studied in this report will focus on the performance of prey-dependent tri-trophic food chains under the influence of the Allee effect [19].

While previous studies primarily focus on the Allee effect, our research extensively examines both the Allee effect and fear effect within a three-trophic-level food chain model. We investigate the impact of bottom-up effects on the system's dynamics, specifically the combined influence of the Allee effect and the fear effect in predator-prey interactions. On the basis of these assumptions, we develop a mathematical model, analyze its equilibria, and assess its stability. Our main contributions are summarized as follows.

- We investigate the Allee effect of a three-trophic-level food chain ecosystem without the fear factor.
- We demonstrate that the Allee effect and the fear effect are crucial for stabilizing the system and analyze their combined impact on the population.
- We integrate the spatial aspect of ecological interactions into the temporal system by extending the ordinary differential equations (ODEs) to a partial differential equation (PDE) framework using reaction-diffusion equations.

The subsequent sections are structured as follows: Section 2 presents some foundational mathematical concepts. Section 3 presents the proposed mathematical model. The analytical results are discussed in Section 4, covering stability conditions, the existence of equilibria, and different bifurcations of two different systems. Section 5 extends the analysis to a special temporal system. Section 6 presents the results of numerical simulations and the global sensitivity analysis. Finally, Section 7 concludes by summarizing the study's significant findings.

The existing models capture either Allee-type thresholds or fear-induced behavioural changes, but seldom both simultaneously. Our proposed system integrates these two mechanisms to better reflect scenarios in which low-density populations experience both cooperative advantages and predator-induced stress. While concrete field applications remain to be explored, this abstraction lays the groundwork for future empirical validation.

2. Preliminaries

In this section, we collect the foundational mathematical concepts and notation necessary for the analysis of the ODE and PDE models presented in subsequent sections.

2.1. Solutions to differential equations

Definition 2.1 (Solution to an ODE)**.** *Let* $\mathbf{u}(t) \in \mathbb{R}^n$ *and consider the initial value problem:*

$$\frac{d\mathbf{u}}{dt} = \mathbf{F}(\mathbf{u}), \quad \mathbf{u}(0) = \mathbf{u}_0. \tag{2.1}$$

A function $\mathbf{u}(t)$ *is said to be a solution on an interval* $[0, T)$ *if it is continuously differentiable and satisfies the equation for all* $t \in [0, T)$*.*

Theorem 1 (Existence and uniqueness (Picard-Lindelöf)). *Let $\mathbf{F} : \mathbb{R}^n \to \mathbb{R}^n$ be Lipschitz continuous. Then, for any initial value $\mathbf{u}_0 \in \mathbb{R}^n$, there is a unique local solution $\mathbf{u}(t)$ to the ODE [20–22].*

Definition 2.2 (Classical and mild solutions for the reaction–diffusion PDE). *Let $\Omega \subset \mathbb{R}^d$ be a bounded domain with a C^2 boundary, $D = diag(d_1, ..., d_n)$ with $d_i > 0$, and $\mathbf{f} : \mathbb{R}^n \to \mathbb{R}^n$ locally Lipschitz. Given $\mathbf{u_0} \in C(\bar{\Omega})^n$, we have*

- *A classical solution $\mathbf{u}$ of*

$$\frac{\partial \mathbf{u}}{\partial t} = D\Delta\mathbf{u} + \mathbf{f}(\mathbf{u}), \quad x \in \Omega,\ t > 0,$$

  satisfies $\mathbf{u} \in C^1([0,T); C(\bar{\Omega}^n)) \cap C([0,T); C^2(\bar{\Omega}^n))$ and the PDE pointwise.
- *A mild solution $\mathbf{u}$ satisfies the variation of constants formula*

$$\mathbf{u}(t) = e^{tD\Delta}\mathbf{u_0} + \int_0^t e^{(t-s)D\Delta}\mathbf{f}(\mathbf{u}(s))ds, \quad t \in [0,T),$$

  where $e^{tD\Delta}$ is the analytic semigroup generated by $D\Delta$ under the chosen boundary condition [23, 24].

Theorem 2 (Well-posedness for reaction–diffusion systems). *Under standard assumptions (e.g., $\mathbf{f}(\mathbf{u})$ Lipschitz in $\mathbf{u}$, $D > 0$), the initial-boundary value problem admits a unique classical solution $\mathbf{u} \in C^1([0,T); C(\bar{\Omega}^n)) \cap C([0,T); C^2(\bar{\Omega}^n))$ or a mild solution $\mathbf{u} \in C([0,T]; L^2(\Omega)^n) \cap L^2(0,T; H_1(\Omega)^n)$ on the time interval $[0,T)$ [25, 26].*

Theorem 3. *(Positivity of the solutions)*

- *In the ODE (2.1), if $\mathbf{u}_0 \in \mathbb{R}^n_{\geq 0}$ and $\mathbf{F}(\mathbf{u})$ is quasi-positive, then the solution $\mathbf{u} \in \mathbb{R}^n_{\geq 0}$ for all intervals of existence.*
- *In the PDE (2.2), if $\mathbf{u}_0 \in \mathbb{R}^n_{\geq 0}$ in Ω, $D > 0$, $\partial_\nu \mathbf{u} = 0$, on $\partial\Omega$, and $\mathbf{f}(\mathbf{u})$ is quasi-positive, then $u_i(x,t) \geq 0$ in Ω for all $t > 0$.*

2.2. Reaction-diffusion operators and Turing instability

- Domain: $\Omega \subset \mathbb{R}$ is a bounded domain with a C^2 boundary $\partial\Omega$.
- Diffusion: The diffusion matrix is diagonal,

$$D = \text{diag}(d_1, ..., d_n) \ \text{ with } \ d_i > 0,$$

  so that each species diffuses independently at rate d_i.
- Boundary conditions: Unless otherwise stated, we impose homogeneous Neumann boundary conditions

$$\partial_\nu \mathbf{u} = 0, \quad \text{on } \partial\Omega,$$

  where ν denotes the outward unit normal. Biologically, this corresponds to zero flux across the boundary, i.e., no migration of individuals across the habitat boundary.
- Initial data: The initial condition $\mathbf{u_0}$ is assumed to be compatible with the boundary conditions i.e., $\partial_\nu \mathbf{u_0} = 0$ on $\partial\Omega$.

Under the assumptions stated above, a general reaction-diffusion system takes the form:

$$\frac{\partial \mathbf{u}}{\partial t} = D\Delta \mathbf{u} + \mathbf{f}(\mathbf{u}), \tag{2.2}$$

where $\mathbf{u} \in \mathbb{R}^n$, D is a diagonal matrix of diffusion coefficients and $\mathbf{f}$ defines the reaction kinetics [27,28].

Definition 2.3 (Turing instability)**.** *An equilibrium* $\mathbf{u}^*$ *is said to be Turing unstable if it is linearly stable in the absence of diffusion but becomes unstable when diffusion is present.*

Turing instability typically arises when the Jacobian matrix $J = D\mathbf{f}(\mathbf{u}^*)$ has all eigenvalues with negative real parts, but the perturbed system with diffusion admits eigenvalues with positive real parts.

2.3. Linear stability and Jacobian matrix

Definition 2.4 (Jacobian matrix)**.** *Given a system of equations* $\mathbf{u}' = \mathbf{f}(\mathbf{u})$*, the Jacobian matrix at* $\mathbf{u}^*$ *is defined as*

$$J(\mathbf{u}^*) = \left[\frac{\partial f_i}{\partial u_j}(\mathbf{u}^*)\right]_{i,j}.$$

Definition 2.5 (Linear stability)**.** *An equilibrium* $\mathbf{u}^*$ *is "linearly stable" if all eigenvalues of* $J(\mathbf{u}^*)$ *have negative real parts; it is "unstable" if at least one eigenvalue has a positive real part.*

The steady-state bifurcations occur when $\det(J) = 0$ with transversality, while Hopf bifurcations occur when $\mathrm{tr}(J) = 0$ and $\det(J) > 0$ (it is for two-dimensional ($2D$) systems). For 3×3 systems, Hopf bifurcations are determined using the Routh–Hurwitz conditions.

Linearization and dispersion relation (Turing). In Definition 2.5, note that $J(\mathbf{u}^*) = D\mathbf{f}(\mathbf{u}^*)$ denotes the Jacobian matrix of the reaction term $\mathbf{f}(\mathbf{u})$ evaluated at the equilibrium $\mathbf{u}^*$. For a reaction-diffusion system (2.2), linearization around $\mathbf{u}^*$ and separation of the variables lead to the dispersion relation,

$$\det\left(\lambda I - J(\mathbf{u}^*) + K^2 D\right) = 0,$$

where k is the spatial wave number and D is the diagonal diffusion matrix. A diffusion-driven instability (Turing instability) requires (i) *ODE-stability*: $\mathrm{Re}(\lambda(0)) < 0$; (ii) *a pattern-forming mode*: $K > 0$ exists such that $\mathrm{Re}(\lambda(K)) > 0$. Notation and standing assumptions for the dimensionless PDE system are presented in Table 1.

These tools will be used throughout the stability, bifurcation, and pattern formation analyses in the following sections.

Table 1. Notation and standing assumptions for the dimensionless PDE system.

Item	Description / Assumption
Spatial domain Ω	Bounded subset of $\mathbb{R}^d$ ($d = 1, 2, 3$) with the smooth boundary $\partial\Omega$.
Boundary conditions	Homogeneous Neumann (no flux): $\frac{\partial x}{\partial \nu} = \frac{\partial y}{\partial \nu} = \frac{\partial z}{\partial \nu} = 0$ on $\partial\Omega$, $\tau > 0$.
Diffusion matrix D	$D = \mathrm{diag}(d_1, d_2, d_3)$ with $d_i > 0$; optional cross-diffusion $d_{ij} \geq 0$ for $i \neq j$.
Reaction term $f(u)$	Given by the right-hand sides of (3.2); C^1 and locally Lipschitz on $\mathbb{R}^3_+$.
Parameter values	All parameters are strictly positive
Initial data	$x(0,\cdot) > 0$, $y(0,\cdot) > 0$, and $z(0,\cdot) > 0$ in Ω; ensures the solution's positivity for all $\tau > 0$.

3. Mathematical model formulation

An ODE involves functions of a single variable and their derivatives. A classical solution is a smooth function satisfying the ODE on a given interval. In population dynamics, ODEs model how species populations change over time according to their growth and interactions [29]. One of the most famous models in this area is the Lotka-Volterra model, which can be described as

$$\begin{aligned} \frac{dx}{dt} &= x(1-x) - \frac{\hat{a}_1 xy}{1+\hat{b}_1 x} \\ \frac{dy}{dt} &= \frac{\hat{a}_1 xy}{1+\hat{b}_1 x} - d_1 y - \frac{\hat{a}_2 yz}{1+\hat{b}_2 y} \\ \frac{dz}{dt} &= \frac{\hat{a}_2 yz}{1+\hat{b}_2 y} - d_2 z, \end{aligned} \tag{3.1}$$

where the initial value of x, y, z should be strictly positive.

However, this model has no contribution to the Allee effect and the intraspecific relationship. Hence, we derive a new model using a multiplicative term involving the Allee constant. Our model's construction is based on the standard Rosenzweig–MacArthur model of tritrophic food chains [4]. However, we do not consider the predators' efficiencies here, and we transfer this assessment into the energy conversion rate, which is more apparent when focusing on the Allee effect on prey. In the prey equation, logistic growth is incorporated to represent the self-regulating increase in the prey population. We note that Allee effects describe reduced individual fitness at low population densities. Specifically, a weak Allee effect implies that the per-capita growth rate declines but remains positive, whereas a strong Allee effect leads to negative growth below a critical threshold [19]. Since the so-called weak Allee effect may result in a reduced growth rate as the population size or density decreases, we consider the following multiplier, which is in the form of $\frac{X}{X+n}$ to represent the discrete logistic model with a weak Allee effect. The positive constant n indicates the strength of the Allee effect. The larger the n, the stronger the effect. This term remains at an increased rate lower than the original logistic equation. Furthermore, the lowest organisms in the food chain are usually producers of some kind, such as grasses, which are generally considered to be the basis of the ecosystem and can be considered to have a much lower death rate than their rate of renewal in the absence of intervention. Thus, we do not consider the death rate of the prey here.

The predator and super-predator are modeled according to the predator part of the traditional model. The Allee effect is only discussed on the prey side in this given model, which could be considered our simulation's foundation. The model is shown below:

$$\begin{aligned} \frac{\mathrm{d}X}{\mathrm{d}t} &= rX(1-\frac{X}{k})\frac{X}{X+n} - m_1 XY \\ \frac{\mathrm{d}Y}{\mathrm{d}t} &= e_1 m_1 XY - m_2 YZ - d_1 Y \\ \frac{\mathrm{d}Z}{\mathrm{d}t} &= e_2 m_2 YZ - d_2 Z, \end{aligned}$$

where $X(t)$, $Y(t)$, and $Z(t)$ stand for the prey density, predator density, and super/top-predator density, respectively; r is a positive number defined as the prey's growth rate; k is the environment capacity;

m_i is used to describe the predatory relationships, standing as the consumption rates; e_i is used to simulate how much of the energy transferred in predatory relationships can be used for reproductive activities, named the conversion rates; d_i is the death rate of two predator species; and n is the Allee effect constant, which represents our research focus. The flow diagram for the baseline methodology is presented in Figure 1. A summary of the model's elements, their characteristics, and their functionalities are presented in Table 2.

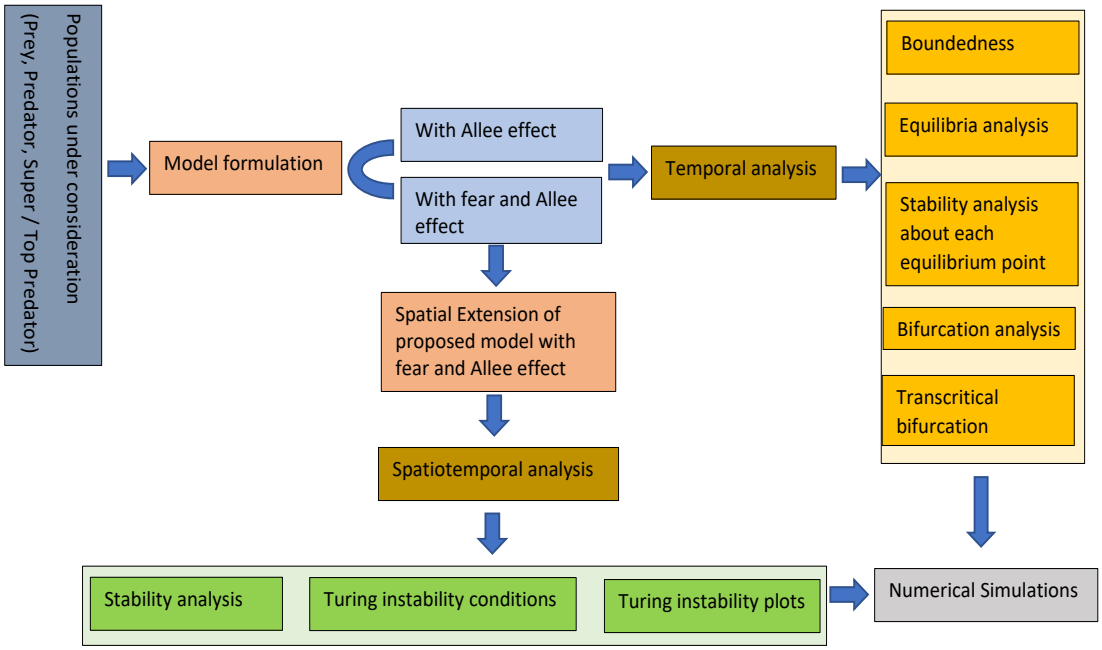

Figure 1. Flow diagram for the baseline methodology.

In this model, it is clear that we have the following assumptions:

- Consider the initial growth sense of view. The prey follows a logistic growth rate combined with the Allee effect.
- The Allee effect is represented and simulated by using the ratio and product of the density of X and related parameters.
- The only cause of the decrease in the prey species is predation in our model.
- The influence of any external activities from spectators is ignored.

In fact, many potential factors influence the Allee effect. The most important cause of the Allee effect is the difficulty of finding mates for individuals in low-density populations. Second, small populations with small yields, low fruiting, food requirements, or dysfunctional group housing are also factors that should not be overlooked as influences [30]. To handle these complicated reasons, we prefer to concentrate on the final output of the Allee effect's influence. Hence, we applied this model,

which summarizes the Allee effect as a simple constant a_1 after nondimensionalization. In many studies, the Allee effect and fear effect are considered jointly [31]. The fear effect has been discussed for years to analyze its influence on stability and the Hopf bifurcation compared with the traditional Holling-type models. Therefore, we modify our previous model by simultaneously analysing the fear and Allee effects on the prey. As this is different from the modeling of the Allee effect, we try to simulate the fear effect with a function $F(f, Y)$, which describes the effect of the predator (Y) on the prey (X) through fear.

In contrast to the classical Allee effect term, we introduce a function $F : \mathrm{Dom(F)} \times \mathrm{Dom(Y)} \to \mathbb{R}^+$, where $f \in \mathbb{R}^+$ measures the fear level and $Y \in \mathrm{Dom(Y)}$ is the predator density. This modifies the prey's growth equation to

$$\frac{\mathrm{d}X}{\mathrm{d}t} = F(f, Y(t))X(t)I(X(t)),$$

where $I : \mathrm{Dom(I)} \to \mathbb{R}^+$ denotes the intrinsic growth rate of the prey.

Definition 3.1 (Fear function)**.** *A function $F : \mathrm{Dom(F)} \times \mathrm{Dom}(Y) \to \mathbb{R}^+$ is called a fear function if, for all $f \in \mathrm{Dom}(F)$ and $Y \in \mathrm{Dom}(Y)$, the following conditions hold:*

(1) $F(f, 0) = F(0, Y) = 1$*;*
(2) $\lim\limits_{f\to\infty} F(f, Y) = \lim\limits_{Y\to\infty} F(f, Y) = 0$*;*
(3) $\dfrac{\partial F}{\partial f}(f, Y) < 0 \quad$ *and* $\quad \dfrac{\partial F}{\partial Y}(f, Y) < 0.$

Remark 1. *As demonstrated in [31], the specific choice*

$$F(f, Y) = \frac{1}{1 + fY}$$

satisfies the conditions above and thus serves as a concrete example.

Hence, this model is shown as follows:

$$\begin{aligned}
\frac{\mathrm{d}X}{\mathrm{d}t} &= \frac{rX}{1 + fY}(1 - \frac{X}{k})\frac{X}{X + n} - m_1XY \\
\frac{\mathrm{d}Y}{\mathrm{d}t} &= e_1m_1XY - m_2YZ - d_1Y \\
\frac{\mathrm{d}Z}{\mathrm{d}t} &= e_2m_2YZ - d_2Z.
\end{aligned}$$

After a similar process nondimensionalization, we get the model

$$\begin{aligned}
\frac{\mathrm{d}x}{\mathrm{d}\tau} &= \frac{x}{1 + \hat{f}y}(1 - x)\frac{x}{x + a_1} - b_1xy \\
\frac{\mathrm{d}y}{\mathrm{d}\tau} &= b_1xy - c_1yz - \hat{d}_1y \\
\frac{\mathrm{d}z}{\mathrm{d}\tau} &= c_1yz - \hat{d}_2z.
\end{aligned} \tag{3.2}$$

The model (3.2) is an ODE system, and its initial conditions are defined as

$$x(0) = x_0 > 0,\ y(0) = y_0 > 0,\ z(0) = z_0 > 0, \tag{3.3}$$

where the dimensionless parameters are roughly similar to the previous factors: $rt = \tau$, $\hat{f} = ke_1 f$, $a_1 = \frac{n}{k}$, $b_1 = \frac{ke_1 m_1}{r}$, $c_1 = \frac{ke_1 e_2 m_2}{r}$, $\hat{d}_1 = \frac{d_1}{r}$, and $\hat{d}_2 = \frac{d_2}{r}$. Wang et al. [31] proved that incorporating a fear effect does not affect the structure of the model's equilibria, which indicates that we still have four types of equilibria, which could be presented as $E_0 = (0, 0, 0)$, $E_1 = (1, 0, 0)$, $E_2 = (x_2, y_2, 0)$, and $E_3 = (x_3, y_3, z_3)$. The details will be analyzed in the next section.

Table 2. Summary of the model's elements with its characteristics and functionalities.

Element	Details
Prey density ($X(t), x$)	Characteristics: Continuous variable; logistic growth with Allee and fear effect. Functionality: Represents base species; affected by growth, fear, and predation.
Predator density ($Y(t), y$)	Characteristics: Intermediate trophic level; consumes prey and is predated upon. Functionality: Gains from prey; loses to super-predator and natural death.
Top predator density ($Z(t), z$)	Characteristics: Apex predator; consumes predators only. Functionality: Top-level consumer; regulated by conversion efficiency and death.
Prey growth rate (r)	Characteristics: Positive constant. Functionality: Governs the intrinsic growth of prey.
Carrying capacity (k)	Characteristics: Maximum sustainable population. Functionality: Limits the prey population's growth.
Allee effect constant (n, $a_1 = \frac{n}{k}$) (Dimensionless)	Characteristics: Controls strength of the Allee effect. Functionality: Suppresses prey growth at a low density.
Fear effect parameter (f, $\hat{f}$)	Characteristics: Non-negative constant. Functionality: Reduces prey growth via predator-induced fear: $F(f, Y) = \frac{1}{1+fY}$.
Prey-predator rate (m_1, $b_1 = \frac{ke_1 m_1}{r}$) (Dimensionless)	Characteristics: Consumption rate. Functionality: Governs rate of prey consumed by predators.
Conversion efficiency predator (e_1)	Characteristics: Fraction of prey biomass converted to predators. Functionality: Influences energy transfer and parameter b_1.
Predator–super-predator rate (m_2, $c_1 = \frac{ke_1 e_2 m_2}{r}$)	Characteristics: Consumption rate. Functionality: Governs rate of predators consumed by top predators.
Conversion efficiency top predator (e_2)	Characteristics: Fraction of predator biomass converted to top predators. Functionality: Influences energy transfer and the parameter c_1.
Death rates (d_1, d_2, $\hat{d}_i = \frac{d_i}{r}$) (Dimensionless)	Characteristics: Natural mortality rates. Functionality: Regulate decline in predator and top predator populations.
Functional response (Holling Type II)	Characteristics: Saturating nonlinear form. Functionality: Used in all predation interactions.
Fear effect function ($F(f, Y) = \frac{1}{1+fY}$)	Characteristics: Decreases with f and Y. Functionality: Modulates prey growth rate caused by predators' presence.
Self-diffusion coefficients (d_1, d_2, d_3)	Characteristics: Positive constants. Functionality: Represent random movement in space.
Cross-diffusion coefficients (d_{12}, d_{21})	Characteristics: Positive constants. Functionality: Capture inter-species driven movement.
Equilibrium points (E_0, E_1, E_2, E_3)	Characteristics: Trivial, boundary, and interior equilibria. Functionality: Used in bifurcation and stability analysis.
Jacobian matrix (J)	Characteristics: Matrix of partial derivatives. Functionality: Used for linearized stability analysis.
Routh-Hurwitz coefficients (A_1, A_2, A_3)	Characteristics: Derived from characteristic polynomials. Functionality: Provide local stability conditions.
Numerical solvers (ode45, dde23, odeint)	Characteristics: Common solvers in MATLAB/Python. Functionality: Used for solving ODEs and simulations.

Proposition 3.1. *(Boundedness) The region*

$$B = \{(x, y, z) : 0 \le W \le \frac{1}{\alpha} + \varepsilon,\ \textit{for any}\ \ \varepsilon{>}0\}$$

contains all solutions of the system (3.2) *as* $t \to \infty$ *for all positive initial values* $(x_0, y_0, z_0) \in \mathbb{R}^3_+$, *where* $\frac{x}{x+a_1} \le 1$ *and* $\alpha = min(1, \hat{d}_1, \hat{d}_2)$.

Proof. Define a positive definite function
$W(\tau) = x + y + z$, which is differentiable in $(0, T)$

$$\begin{aligned} \frac{dW}{d\tau} &= \frac{dx}{d\tau} + \frac{dy}{d\tau} + \frac{dz}{d\tau} \\ &= x(1-x)\frac{x}{x+a_1} - \hat{d}_1 y - \hat{d}_2 z \\ &= [x(1-x)\frac{x}{x+a_1} + x] - x - \hat{d}_1 y - \hat{d}_2 z \\ \frac{dW}{d\tau} + x + \hat{d}_1 y + \hat{d}_2 z &= x(1-x)\frac{x}{x+a_1} + x. \end{aligned} \tag{3.4}$$

Then, by $\frac{x}{x+a_1} \leq 1$ and $\alpha = min(1, \hat{d}_1, \hat{d}_2)$, we can see that

$$\begin{aligned} &\frac{dW}{d\tau} + \alpha W \leq -(x-1)^2 + 1 \\ &\frac{dW}{d\tau} + \alpha W \leq 1 \\ &0 \leq W \leq \frac{1}{\alpha} + ce^{-\alpha\tau} \\ &0 \leq W \leq \frac{1}{\alpha} + e^{-\alpha\tau}(W_0 - \frac{1}{\alpha}) \\ &0 \leq W \leq \frac{1}{\alpha}(1 - e^{-\alpha\tau}) + e^{-\alpha\tau} W_0, \end{aligned} \tag{3.5}$$

where $c = W_0 - \frac{1}{\alpha}$, and for $\tau \to +\infty$, $0 \leq W \leq \frac{1}{\alpha}$. Thus, all the solutions belong to $B = \{(x, y, z) : 0 \leq W \leq \frac{1}{\alpha} + \varepsilon$, for any ε>0$\}$. □

4. Stability and bifurcation analysis

The analysis of equilibrium points is fundamental in understanding the long-term behavior of ecological systems. In particular, equilibria represent steady states where population densities remain constant over time. By studying their existence and stability, we gain insight into key ecological questions such as the following.

- **Persistence:** Under what conditions do all species coexist indefinitely?
- **Extinction:** Are there scenarios where one or more species go extinct?
- **Bifurcations:** How do qualitative changes in the system's dynamics arise as the parameters vary (e.g., Allee threshold, predation rate)?

Local stability analysis near each equilibrium helps determine whether small perturbations will decay (stability) or grow (instability), thereby guiding the prediction of species' survival, outbreak, or collapse. Furthermore, the occurrence of bifurcation points—such as saddle-node or Hopf bifurcations—marks critical thresholds where the system's behavior changes dramatically, often leading to complex dynamics such as oscillations or pattern formation.

Equilibrium points represent steady states of the system and provide crucial insight into species' persistence, extinction, and bifurcation behavior. Analyzing their stability helps determine whether populations return to equilibrium after small disturbances or diverge toward alternate dynamics such as collapse or oscillation. This analysis also reveals critical thresholds—bifurcation points—beyond which qualitative changes occur in the system's behavior.

To study local stability, we linearize the system near an equilibrium $E^* = (X^*, Y^*, Z^*)$ by computing the Jacobian matrix:

$$J(X,Y,Z) = \frac{\partial(f,g,h)}{\partial(X,Y,Z)} = \begin{bmatrix} \frac{\partial f}{\partial X} & \frac{\partial f}{\partial Y} & \frac{\partial f}{\partial Z} \\ \frac{\partial g}{\partial X} & \frac{\partial g}{\partial Y} & \frac{\partial g}{\partial Z} \\ \frac{\partial h}{\partial X} & \frac{\partial h}{\partial Y} & \frac{\partial h}{\partial Z} \end{bmatrix},$$

where (f, g, h) denote the right-hand sides of the system (3.2). The eigenvalues of J evaluated at E^* determine the local stability: All eigenvalues with negative real parts imply asymptotic stability, while any positive real part indicates instability.

4.1. Equilibrium points and stability of the system (3.2) *without fear*

Definition 4.1. *(Equilibrium) A point* $E = (X^*, Y^*, Z^*)$ *is an equilibrium of the system* (3.2) *if* $(f, g, h)(X^*, Y^*, Z^*) = (0, 0, 0)$.

The following equilibrium points can be found:
(i) *Trivial equilibrium*: $E_0 = (0, 0, 0)$;
(ii) *Axial equilibrium*: $E_1 = (1, 0, 0)$;
(iii) *Boundary equilibrium*: $E_2 = (x_2, y_2, 0)$, where $x_1 = \frac{\hat{d}_1}{b_1}$ and $y_2 = \frac{\hat{d}_1(b_1-\hat{d}_1)}{(\hat{d}_1+a_1b_1)b_1^2}$.
(iv) *Coexistence equilibrium*: $E_3 = (x_3, y_3, z_3)$, where (x_3, y_3, z_3) satisfies the relation:

$$x_3^2 + \left(\frac{b_1\hat{d}_2}{c_1} - 1\right)x_3 + \frac{a_1b_1\hat{d}_2}{c_1} = 0; y_3 = \frac{\hat{d}_2}{c_1}; z_3 = \frac{b_1x_3 - \hat{d}_1}{c_1}. \tag{4.1}$$

Explicitly, the Jacobian matrix at the equilibrium $\bar{E} = (\bar{x}, \bar{y}, \bar{z})$ can be defined by

$$\bar{V} = \begin{bmatrix} \bar{j}_{11} & \bar{j}_{12} & 0 \\ \bar{j}_{21} & \bar{j}_{22} & \bar{j}_{23} \\ 0 & \bar{j}_{32} & \bar{j}_{33} \end{bmatrix},$$

$\bar{j}_{11} = \frac{2\bar{x}-3\bar{x}^2-b\bar{x}\bar{y}}{\bar{x}+a_1} - b\bar{y}$, $\bar{j}_{12} = -b_1\bar{x}$, $\bar{j}_{13} = 0$, $\bar{j}_{21} = b_1\bar{y}$, $\bar{j}_{22} = b_1\bar{x} - c_1\bar{z} - \hat{d}_1$, $\bar{j}_{23} = -c_1\bar{y}$, $\bar{j}_{31} = 0$, $\bar{j}_{32} = c_1\bar{z}$, $\bar{j}_{33} = c_1\bar{y} - \hat{d}_2$.

Behaviors of E_0

The eigenvalues for E_0 are $\lambda_1 = 0$, $\lambda_2 = -\hat{d}_1$, $\lambda_3 = -\hat{d}_2$; one eigenvalue is zero and other two eigenvalues are negative. Therefore, the equilibrium point E_0 is marginally stable.

Behaviors of E_1

The eigenvalues for E_1 are $\lambda_1 = \frac{-1}{1+a_1} < 0$, $\lambda_2 = b_1 - \hat{d}_1$, $\lambda_3 = -\hat{d}_2 < 0$. Therefore, the equilibrium point E_1 is locally asymptotically stable only if $b_1 < \hat{d}_1$.

Behaviors of E_2

The Jacobian matrix at point $E_2 = (x_2, y_2, 0)$ where $x_2 = \frac{\hat{d}_1}{b_1}$ and $y_2 = \frac{\hat{d}_1(b_1-\hat{d}_1)}{(\hat{d}_1+ab_1)b_1^2}$ is given by

$$M_1 = \begin{pmatrix} \check{m}_{11} & -b_1x_2 & 0 \\ b_1y_2 & 0 & -c_1y_2 \\ 0 & 0 & c_1y_2 - \hat{d}_2 \end{pmatrix},$$

in which $\check{m}_{11} = \frac{2x_2-3x_2^2-b_1x_2y_2}{x_2+a_1} - b_1y_2$.

If $c_1y_2 - \hat{d}_2 \le 0$ and $\check{m}_{11} \le 0$, then $T = \check{m}_{11} + 0 + c_1y_2 - \hat{d}_2 < 0$ and $D = (c_1y_2 - \hat{d}_2)b_1x_2b_1y_2 < 0$.

By assuming $c_1y_2 - \hat{d}_2 \le 0$ and $\check{m}_{11} \le 0$, we can find that $y_2 \le \frac{\hat{d}_2}{c_1}$ and $y_2 > \frac{2x_2-3x_2^2}{2b_1x_2+a_1b_1}$. From $y_2 = \frac{\hat{d}_1(b_1-\hat{d}_1)}{(\hat{d}_1+a_1b_1)b_1^2} = A$, we conclude that:

$$\begin{aligned} &3x_2^2 - 2x_2 + 2Ab_1x_2 + a_1b_1A > 0, \\ &x_{21} = \frac{1 - Ab_1 + \sqrt{(Ab_1-1)^2 - 3a_1b_1A}}{3}, \\ &x_{22} = \frac{1 - Ab_1 - \sqrt{(Ab_1-1)^2 - 3a_1b_1A}}{3}. \end{aligned} \tag{4.2}$$

As $x_{21} < \frac{1-Ab_1+|Ab_1-1|}{3}$, if $Ab_1 - 1 > 0$, then $x_2 < 0$; if $Ab_1 - 1 < 0$, then $x_2 < \frac{2(1-Ab_1)}{3}$. Hence, the system is locally asymptotically stable around the equilibrium point E_2 only if $x_2 < \frac{2(1-Ab_1)}{3}$, $y_2 < \frac{\hat{d}_2}{c_1}$, for which $Ab_1 - 1 < 0$.

Behaviors of E_3

(x_3, y_3, z_3) satisfies the relation

$$x_3^2 + (\frac{b_1\hat{d}_2}{c_1} - 1)x_3 + \frac{a_1b_1\hat{d}_2}{c_1} = 0,\ y_3 = \frac{\hat{d}_2}{c_1},\ z_3 = \frac{b_1x_3 - \hat{d}_1}{c_1}. \tag{4.3}$$

The Jacobian matrix M_3 around the equilibrium point E_3 is given by $M_3 = (m_{ij})_{33}$, where $m_{11} = \frac{2x_3-3x_3^2-b_1x_3y_3}{x_3+a_1} - b_1y_3$, $m_{12} = -b_1x_3 < 0$, $m_{13} = 0$, $m_{21} = b_1y_3 > 0$, $m_{22} = b_1x_3 - c_1z_3 - \hat{d}_1 = 0$, $m_{23} = -c_1y_3 < 0$, $m_{31} = 0$, $m_{32} = c_1z_3 > 0$, and $m_{33} = c_1y_3 - \hat{d}_2 = 0$. Let λ_i be the roots of the characteristic equation of M_3 where $i = 1, 2, 3$

$$\begin{aligned} &\lambda^3 + A_1\lambda^2 + A_2\lambda + A_3 = 0, \\ &A_1 = -m_{11},\ A_2 = -(m_{12}m_{21} + m_{23}m_{32}),\ A_3 = m_{11}m_{23}m_{32}. \end{aligned} \tag{4.4}$$

From the Routh–Hurwitz criterion, E_3 is locally asymptotically stable if and only if $A_1 > 0$, $A_3 > 0$ and $A_1A_2 > A_3$. Hence, we have

$$A_1A_2 - A_3 = m_{11}m_{12}m_{21}. \tag{4.5}$$

Since $m_{12} < 0$, $m_{21} > 0$, if $m_{11} < 0$, we can obtain $A_1A_2 - A_3 > 0$ because $A_1A_2 - A_3 = m_{11}m_{12}m_{21}$. Moreover, the necessary condition for $A_1 > 0$ and $A_3 > 0$ is $m_{11} < 0$. As a result

$$\begin{aligned}
&\frac{2x_3 - 3x_3^2 - b_1x_3y_3}{x_3 + a_1} - b_1y_3 < 0, \quad \Rightarrow 2x_3 - 3x_3^2 - b_1x_3y_3 < (x_3 + a_1)b_1y_3,\\
&y_3 = \frac{\hat{d}_2}{c_1},\ 3x_3^2 + (\frac{2b_1\hat{d}_2}{c_1} - 2)x_3 + \frac{a_1b_1\hat{d}_2}{c_1} > 0,\\
&x_{31} = \frac{1 - \frac{b_1\hat{d}_2}{c_1} - \sqrt{(\frac{b_1\hat{d}_2}{c_1} - 1)^2 - \frac{3a_1b_1\hat{d}_2}{c_1}}}{3},\ x_{32} = \frac{1 - \frac{b_1\hat{d}_2}{c_1} + \sqrt{(\frac{b_1\hat{d}_2}{c_1} - 1)^2 - \frac{3a_1b_1\hat{d}_2}{c_1}}}{3},
\end{aligned} \tag{4.6}$$

Here $\frac{1-\frac{b_1\hat{d}_2}{c_1} + \sqrt{(\frac{b_1\hat{d}_2}{c_1}-1)^2 - \frac{3a_1b_1\hat{d}_2}{c_1}}}{3} < \frac{1-\frac{b_1\hat{d}_2}{c_1} + \left|\frac{b_1\hat{d}_2}{c_1}-1\right|}{3}$, if $\frac{b_1\hat{d}_2}{c_1} - 1 > 0$, then $x < 0$, if $\frac{b_1\hat{d}_2}{c_1} - 1 < 0$, then $x < \frac{2(1-\frac{b_1\hat{d}_2}{c_1})}{3}$. Hence, the system is locally asymptotically stable around the point E_3 only if $x < \frac{2(1-\frac{b_1\hat{d}_2}{c_1})}{3}$.

4.2. Bifurcation analysis of the system (3.2) *without fear*

4.2.1. Bifurcation analysis of E_1

By considering the given model (which only has the Allee effect, not the fear effect), the Jacobian is:

$$N_1 = \begin{pmatrix} \frac{-1}{1+a_1} & -b_1 & 0 \\ 0 & b_1 - \hat{d}_1 & 0 \\ 0 & 0 & -\hat{d}_2 \end{pmatrix}.$$

The eigenvalues are calculated by the following equation:

$$\det(N_1 - \lambda I) = 0. \tag{4.7}$$

We then get $\lambda_1 = \frac{-1}{1+a_1}$, $\lambda_2 = b_1 - \hat{d}_1$, $\lambda_3 = -\hat{d}_2$. N_1 has a zero eigenvalue if and only if $det(N_1) = 0$, which provides $b_1 - \hat{d}_1 = 0$, which means that $b_1 = \hat{d}_1$.

Let v and ϕ be the eigenvectors corresponding to N_1 and N_1^T (the transpose of N_1) when the eigenvalue equals 0. Therefore, we obtain $v = (v_1, v_2, 0)^T$ and $\phi = (0, \phi_2, 0)^T$ where $v_2 = \frac{-v_1}{b_1(1+a_1)}$ and v_1, ϕ_2 are any two nonzero real numbers.

E_1 according to the parameter b_1

By calculating $\phi^T[F_{b_1}(E_1, b_1^*)] = 0$, where $b_1^* = \hat{d}_1$, it can be seen that the system does not have any saddle-node bifurcation. Moreover,

$$DF_{b_1}(E_1, b_1^*) = \begin{pmatrix} 0 & -1 & 0 \\ 0 & -1 & 0 \\ 0 & 0 & 0 \end{pmatrix},$$

$$D^2F(E_1, b_1^*) = \begin{pmatrix} \frac{-2-4a_1}{(1+a_1)^2} & -\hat{d}_1 & 0 \\ \hat{d}_1 & 0 & -c_1 \\ 0 & c_1 & 0 \end{pmatrix}.$$

Furthermore,

$$D^2F(E_1, b_1^*)(v, v) = \begin{pmatrix} \frac{-2-4a_1}{(1+a_1)^2} v_1^2 - 2b_1^* v_1 v_2 \\ 2b_1^* v_1 v_2 \\ 0 \end{pmatrix}.$$

By calculating $\phi^T[DF_{b_1}(E_1, b_1^*)v] \neq 0$ and $\phi^T[D^2F(E_1, b_1^*)(v, v)] \neq 0$, we find that the system possesses a transcritical bifurcation.

E_1 according to the parameter $\hat{d}_1$

By calculating $\phi^T[F_{\hat{d}_1}(E_1, \hat{d}_1^*)] = 0$, where $\hat{d}_1^* = b_1$, it can be seen that the system does not have any saddle-node bifurcation. In addition,

$$DF_{\hat{d}_1}(E_1, \hat{d}_1^*) = \begin{pmatrix} 0 & 0 & 0 \\ 0 & -1 & 0 \\ 0 & 0 & 0 \end{pmatrix},$$

$$D^2F(E_1, \hat{d}_1^*) = \begin{pmatrix} \frac{-2-4a_1}{(1+a_1)^2} & -\hat{d}_1^* & 0 \\ \hat{d}_1^* & 0 & -c_1 \\ 0 & c_1 & 0 \end{pmatrix}.$$

Therefore, we get

$$D^2F(E_1, \hat{d}_1^*)(v, v) = \begin{pmatrix} \frac{-2-4a_1}{(1+a_1)^2} v_1^2 - 2b_1 v_1 v_2 \\ 2b_1 v_1 v_2 \\ 0 \end{pmatrix}.$$

By calculating $\phi^T[DF_{d_1}(E_1, \hat{d}_1^*)v] \neq 0$ and $\phi^T[D^2F(E_1, \hat{d}_1^*)(v, v)] \neq 0$, we find that the system possesses a transcritical bifurcation.

4.2.2. Bifurcation analysis of E_2

The Jacobian matrix at the point $E_2 = (x_2, y_2, 0)$ where $x_2 = \frac{\hat{d}_1}{b_1}$ and $y_2 = \frac{\hat{d}_1(b_1-\hat{d}_1)}{(\hat{d}_1+ab_1)b_1^2}$ is given by

$$M_1 = \begin{pmatrix} n_{11} & -b_1x_2 & 0 \\ b_1y_2 & 0 & -c_1y_2 \\ 0 & 0 & c_1y_2 - \hat{d}_2 \end{pmatrix},$$

where $n_{11} = \frac{2x_2-3x_2^2-b_1x_2y_2}{x_2+a} - b_1y_2$, and the eigenvalues are calculated by the following equation:

$$det(M_1 - \lambda I) = 0. \tag{4.8}$$

The eigenvalues are

$$\lambda_{1,2} = \frac{1}{2}\Big[(n_{11}) \pm \sqrt{n_{11}^2 + 4(-b_1x_2)(b_1y_2)}\Big],\ \lambda_3 = \frac{c\hat{d}_1(b_1-\hat{d}_1)}{(\hat{d}_1+a_1b_1)b_1^2} - \hat{d}_2. \tag{4.9}$$

Let u and ϕ be the eigenvectors corresponding to M_1 and M_1^T (the transpose of M_1) when the eigenvalue equals 0. Therefore, we obtain $u = (u_1, u_2, u_3)^T$ and $\phi = (0, 0, \phi_3)^T$ where $u_1 = \frac{c_1u_3}{b_1}$, $u_2 = \frac{n_{11}c_1u_3}{\hat{d}_1b_1}$ and u_3, ϕ_3 are any two nonzero real numbers.

E_2 according to the parameter a_1

The system experiences a Hopf bifurcation around E_2 at $a_1 = a_1^*$ where $a_1^* = \frac{2x_2-3x_2^2-2b_1x_2y_2}{b_1y_2}$.

$\lambda_{1,2}$ is purely imaginary if and only if $n_{11} = 0$, which leads to $a_1 = a_1^*$. Next, we obtain $Re\Big(\frac{d\lambda_i}{da_1}\Big)_{a_1=a_1^*} = -\frac{b_1y_2}{2(x_2+a_1^*)} \neq 0, i = 1, 2.$

Therefore, the Hopf bifurcation occurs near E_2 for $a_1 = a_1^*$.

E_2 according to the parameter b_1

With a similar method, we check that the system also experiences a Hopf–bifurcation around E_2 with $b_1 = b_1^*$ where $b_1^* = \frac{2x_2-3x_2^2}{2x_2y_2+y_2a_1}$. Since the value $Re\Big(\frac{d\lambda_i}{db_1}\Big)_{b_1=b_1^*} = -\frac{3x_2y_2+2y_2a_1}{2(x_2+a_1)^2} \neq 0$, $i = 1, 2$ can be obtained, the conclusion can be drawn that the Hopf bifurcation occurred at $b_1 = b_1^*$ around the point E_2.

E_2 according to the parameter c_1

By calculating $\phi^T[F_{c_1}(E_2, c_1^*)] = 0$, where $c_1^* = \frac{(\hat{d}_1+a_1b_1)b_1^2\hat{d}_2}{\hat{d}_1(b_1-\hat{d}_1)}$, the system does not reach saddle-node bifurcation around E_2 at $c_1 = c_1^*$. Moreover,

$$DF_{c_1}(E_2, c_1^*) = \begin{pmatrix} 0 & 0 & 0 \\ 0 & 0 & y_1 \\ 0 & 0 & y_1 \end{pmatrix}.$$

Hence, $\phi^T[DF_{c_1}(E_2, c_1^*)u] = \phi_3 y_1 u_3 \neq 0$.

$$D^2F(E_2, c_1^*) = \begin{pmatrix} \frac{\partial^2 F_1}{\partial x^2}\Big|_{x_2} & -b_1 & 0 \\ b_1 & 0 & -c_1^* \\ 0 & c_1^* & 0 \end{pmatrix},$$

$$D^2F(E_2, c_1^*)(u,u) = \begin{pmatrix} \frac{\partial^2 F_1}{\partial x^2}\Big|_{x_2} u_1^2 - 2b_1 u_1 u_2 \\ 2b_1 u_1 u_2 - 2c_1^* u_2 u_3 \\ 2c_1^* u_2 u_3 \end{pmatrix}.$$

Therefore, $\frac{\partial^2 F_1}{\partial x^2}\Big|_{x_2} = \frac{2-6x_2}{x_2+a_1} + \frac{2(3x_2^2-2x_2)}{(x_2+a_1)^2} + \frac{2(x_2^2-x_2^3)}{(x_2+a_1)^3}$. Hence, $\phi^T[D^2F(E_2, c_1^*)(u,u)] = 2\phi_3 c_1^* u_2 u_3 \neq 0$. Therefore, the system experiences a transcritical bifurcation at $c_1 = c_1^*$ around the equilibrium E_2.

E_2 according to the parameter $\hat{d}_2$

By calculating $\phi^T[F_{\hat{d}_2}(E_2, \hat{d}_2{}^*)] = 0$, where $\hat{d}_2{}^* = \frac{c_1\hat{d}_1(b_1-\hat{d}_1)}{(\hat{d}_1+a_1b_1)b_1^2}$, the system does not attain saddle-node bifurcation around E_2 at $\hat{d}_2 = \hat{d}_2{}^*$. Moreover,

$$DF_{\hat{d}_2}(E_2, \hat{d}_2{}^*) = \begin{pmatrix} 0 & 0 & 0 \\ 0 & 0 & 0 \\ 0 & 0 & -1 \end{pmatrix}.$$

Hence, $\phi^T[DF_{\hat{d}_2}(E_2, \hat{d}_2{}^*)u] = -\phi_3 u_3 \neq 0$.

$$D^2F(E_2, \hat{d}_2{}^*) = \begin{pmatrix} \frac{\partial^2 F_1}{\partial x^2}\Big|_{x_1} & -b_1 & 0 \\ b_1 & 0 & -c_1 \\ 0 & c_1 & 0 \end{pmatrix},$$

$$D^2F(E_2, \hat{d}_2{}^*)(u,u) = \begin{pmatrix} \frac{\partial^2 F_1}{\partial x^2}\Big|_{x_2} u_1^2 - 2b_1 u_1 u_2 \\ 2b_1 u_1 u_2 - 2c_1 u_2 u_3 \\ 2c_1 u_2 u_3 \end{pmatrix}.$$

Therefore, $\frac{\partial^2 F_1}{\partial x^2}\Big|_{x_2} = \frac{2-6x_2}{x_2+a_1} + \frac{2(3x_2^2-2x_2)}{(x_2+a_1)^2} + \frac{2(x_2^2-x_2^3)}{(x_2+a_1)^3}$. Hence, $\phi^T[D^2F(E_2, \hat{d}_2{}^*)(u,u)] = 2\phi_3 c_1 u_2 u_3 \neq 0$. Thus the system experiences transcritical bifurcation at $\hat{d}_2 = \hat{d}_2{}^*$ around the equilibrium E_2.

4.2.3. Bifurcation analysis of E_3

E_3 according to the parameter a_1

First, we consider the given model (which only has the Allee effect, not the fear effect). The Jacobian is

$$J_1 = \begin{pmatrix} m_{11} & -b_1x_3 & 0 \\ b_1y_3 & m_{22} & -c_1y_3 \\ 0 & c_1z_3 & m_{33} \end{pmatrix}$$

where

$$m_{11} = \frac{(2x_3 - 3x_3^2)(x_3 + a_1) + x_3^3 - x_3^2}{(x_3 + a_1)^2};\ m_{22} = b_1x_3 - c_1z_3 - \hat{d}_1 = 0;\ m_{33} = c_1y_3 - \hat{d}_2 = 0. \tag{4.10}$$

The characteristic equation can be formed as follows:

$$(m_{11} - \lambda)[\lambda^2 - m_{23}m_{32}] + m_{12}m_{21}\lambda = 0,$$

which could be simplified to

$$A - B = 0,$$

where

$$A = [-\lambda^3 + m_{11}\lambda^2 + m_{12}m_{21}\lambda],\ B = (m_{11} - \lambda)m_{23}m_{32}. \tag{4.11}$$

In terms of the parameter a_1, we can conclude that:

$$\lambda_{1,2} = \frac{1}{2}\Big[m_{11} \pm \sqrt{m_{11}^2 + 4m_{12}m_{21})}\Big]. \tag{4.12}$$

According to the actual value of m_{ij}, it is clear that λ_1 and λ_2 will be pure imaginary if and only if there is an $a_1 = a_1^{[hbE_3]}$ in which $a_1^{[hbE_3]}$ satisfies the following equation:

$$\Omega + \Delta = b_1(a_1^{[hbE_3]} + x_3)^2(x_3 - y_3). \tag{4.13}$$

This comes from $m_{11} + m_{22} = 0$, where

$$\Omega = (a_1^{[hbE_3]})^2c_1z_3 + a_1^{[hbE_3]}x_3(2c_3z_3 + 3x_3 - 2),\ \Delta = \hat{d}_2(a_1^{[hbE_3]} + x_3)^2 + x_3^2(c_1z_3 + 2x_3 - 1). \tag{4.14}$$

$\frac{\partial(m_{11}+m_{22})}{\partial a_1} \neq 0$ means a Hopf bifurcation exists around E_3.

E_3 according to the parameter b_1

In terms of the bifurcation analysis depending on the parameter b_1, we can summarize the following process. Recall that $E_3(x_3, y_3, z_3)$ satisfies the relation

$$\begin{aligned} &x_3^2 + (\frac{b_1\hat{d}_2}{c_1} - 1)x_3 + \frac{a_1 b_1 \hat{d}_2}{c_1} = 0,\ x_3 \geq \frac{\hat{d}_1}{b_1},\ x_3 \leq \frac{1}{2}, \\ &y_3 = \frac{\hat{d}_2}{c_1} \qquad\qquad \Rightarrow m_{33} = 0, \\ &z_3 = \frac{b_1 x_3 - \hat{d}_1}{c_1} \qquad \Rightarrow m_{22} = 0. \end{aligned} \tag{4.15}$$

It is clear that the only way to have $\lambda = 0$ (which is required when analyzing the type of bifurcation) is to have $m_{11} = m_{33} = \lambda = 0$. Under this condition, plugging E_3 into J_1 will obtain the matrix J_2

$$J_2 = \begin{pmatrix} 0 & -b_1 x_3 & 0 \\ \frac{b_1\hat{d}_2}{c_1} & 0 & -\hat{d}_2 \\ 0 & b_1 x_3 - \hat{d}_1 & 0 \end{pmatrix}.$$

According to Sotomayor's theorem of saddle-node bifurcation, the corresponding eigenvector $\overrightarrow{V(E_3)}$ is required to satisfy the following form of linear algebra:

$$\begin{pmatrix} 0 & -b_1 x_3 & 0 \\ \frac{b_1\hat{d}_2}{c_1} & 0 & -\hat{d}_2 \\ 0 & b_1 x_3 - \hat{d}_1 & 0 \end{pmatrix} \begin{pmatrix} V(E_3)_1 \\ V(E_3)_2 \\ V(E_3)_3 \end{pmatrix} = \mathbf{0}. \tag{4.16}$$

Hence, we have:

$$\overrightarrow{V(E_3)} = \begin{pmatrix} V(E_3)_1 \\ 0 \\ \frac{b_1}{c_1} V(E_3)_1 \end{pmatrix}. \tag{4.17}$$

We then move on to the J_2^T and find its corresponding eigenvector $\overrightarrow{\omega(E_3)}$ and repeat the previous operations, given that J_2^T is in the following form:

$$J_2^T = \begin{pmatrix} 0 & \frac{b_1\hat{d}_2}{c_1} & 0 \\ -b_1 x_3 & 0 & b_1 x_3 - \hat{d}_1 \\ 0 & -\hat{d}_2 & 0 \end{pmatrix}.$$

Hence, we get

$$\overrightarrow{\omega(E_3)} = \begin{pmatrix} \omega(E_3)_1 \\ 0 \\ \frac{b_1 x_3}{b_1 x_3 - \hat{d}_1} \omega(E_3)_1 \end{pmatrix}. \tag{4.18}$$

It is proved that $\omega^T F_{b_1} \neq 0$, given that $\frac{\partial \overrightarrow{F}}{\partial b_1}$ (the partial derivative of the original ODEs depending on the parameter b_1) is

$$\overrightarrow{F_{b_1}} = \begin{pmatrix} -xy \\ xy \\ 0 \end{pmatrix}. \tag{4.19}$$

Also, the $D^2\overrightarrow{F}(x_3, y_3, z_3, b_1)(V(E_3), V(E_3))$ is calculated in the form below according to Perko [22]. It can be simplified if we let e_3 represent the $\frac{\partial^2 F_1}{\partial x^2}$, which is equal to $\hat{C} - \hat{D}$, where

$$\hat{C} = \frac{\left(6x^2 + (2 - 6a_1)x + 2a_1\right)(x + a_1)}{(x + a_1)^3},\ \hat{D} = \frac{2\left(-2x^3 + (1 - 3a_1)x^2 + 2a_1 x\right)}{(x + a_1)^3}. \tag{4.20}$$

The simplified form is like this:

$$D^2\overrightarrow{F}(x_3, y_3, z_3, b_1)(V(E_3), V(E_3)) = \begin{pmatrix} e_3\big|_{x_3} \\ 0 \\ 0 \end{pmatrix}. \tag{4.21}$$

Hence, once $e_3\big|_{x_3} \neq 0$, this will form a saddle-node bifurcation.

E_3 according to the parameter c_1

We now consider the parameter c_1. As b_1 and c_1 are both energy utilization ratios, they affect the model in similar ways. We therefore follow the same steps as we did when analyzing b_1, where the first difference happens in $\overrightarrow{F_{c_1}}$

$$\overrightarrow{F_{c_1}} = \begin{pmatrix} 0 \\ -yz \\ yz \end{pmatrix}. \tag{4.22}$$

With the same eigenvectors $\vec{V}, \vec{\omega}$ for J_2^T, J_2, it is obvious to see that $\omega^T\overrightarrow{F_{c_1}} \neq 0$. Since $\vec{\omega_2}$ is zero, the answer to this multiplication is $\vec{\omega_3} y_3$, which is not zero.

Next, we can find the existence of saddle-bifurcation based on the parameter c_1 by the same method used to analyze b_1.

E_3 according to the parameter $\hat{d_2}$

By the same method, we find that the saddle-node bifurcation exists, based on parameter $\hat{d_2}$, where $\overrightarrow{F_{c_1}}$ is obtained

$$\overrightarrow{F_{\hat{d_2}}} = \begin{pmatrix} 0 \\ 0 \\ -z \end{pmatrix}. \tag{4.23}$$

4.3. Equilibrium points and stability analysis of the system (3.2) *with fear*

The following equilibrium points can be found: Trivial equilibrium: $E_0 = (0, 0, 0)$. Axial equilibrium: $E_1 = (1, 0, 0)$. Boundary equilibrium: $\hat{E}_2 = (\hat{x}_2, \hat{y}_2, 0)$,
where $\hat{x}_2 = \frac{\hat{d}_1}{b_1}, \hat{y}_2 = \frac{b_1\sqrt{a_1b_1+\hat{d}_1}\sqrt{a_1b_1^3+4b_1\hat{d}_1\hat{f}+b_1^2\hat{d}_1-4\hat{d}_1^2\hat{f}}-a_1b_1^3-b_1^2\hat{d}_1}{2\left(a_1b_1^3\hat{f}+b_1^2\hat{d}_1\hat{f}\right)}$.

Positive interior equilibrium: $\hat{E}_3 = (\hat{x}_3, \hat{y}_3, \hat{z}_3)$,
where $\hat{x}_3 = \frac{\sqrt{L}-b_1c_1\hat{d}_2-b_1\hat{d}_2^2\hat{f}+c_1^2}{2c_1^2}, \hat{y}_3 = \frac{\hat{d}_2}{c_1}, \hat{z}_3 = \frac{\frac{b_1\sqrt{L}}{c_1^2}-\frac{b_1^2\hat{d}_2^2\hat{f}}{c_1^2}-\frac{b_1^2\hat{d}_2}{c_1}+b_1-2\hat{d}_1}{2c_1}$, and
$L = \left(b_1c_1\hat{d}_2 + b_1\hat{d}_2^2\hat{f} - c_1^2\right)^2 - 4c_1^2\left(a_1b_1c_1\hat{d}_2 + a_1b_1\hat{d}_2^2\hat{f}\right)$. Here, $\hat{E}_3$ exists if $\hat{x}_3 > 0, \hat{y}^3 > 0, \hat{z}_3 > 0$ depends upon the system's parameters. Explicitly, the Jacobian matrix at $\bar{E} = (\bar{x}, \bar{y}, \bar{z})$ can be defined as

$$\bar{J} = \begin{pmatrix} \frac{\bar{x}\left(-2\bar{x}^2+\bar{x}+(2-3\bar{x})a_1\right)}{(\hat{f}\bar{y}+1)(\bar{x}+a_1)^2} - \bar{y}b_1 & \bar{x}\left(\frac{\hat{f}(\bar{x}-1)\bar{x}}{(\hat{f}\bar{y}+1)^2(\bar{x}+a_1)} - b_1\right) & 0 \\ \bar{y}b_1 & \bar{x}b_1 - \bar{z}c_1 - \hat{d}_1 & -\bar{y}c_1 \\ 0 & \bar{z}c_1 & \bar{y}c_1 - \hat{d}_2 \end{pmatrix}. \tag{4.24}$$

4.3.1. Transcritical bifurcation

Proposition 4.1. *When b_1 surpasses the critical threshold b_1^{TC}, the system* (3.2) *experiences a transcritical bifurcation.*

Proof. At $\hat{E}_1$, the Jacobian matrix $J_{\hat{E}_1}$ of the system (3.2) exhibits a single eigenvalue, becoming zero when $b_1 = b_1^{TC}$. Let U_1 and V_1 be the eigenvectors associated with the eigenvalue zero of the matrices J_{E_1} and $J_{E_1}^T$, respectively. They are defined as follows: $U_1 = \left(-\frac{\hat{\Pi}_{12}}{\hat{\Pi}_{11}} \;\; 1 \;\; 0\right)^T$ and $V_1 = (0 \;\; 1 \;\; 0)^T$. Let $F(x, y, z) = \begin{pmatrix} f_1(x,y,z) & f_2(x,y,z) & f_3(x,y,z) \end{pmatrix}^T$. Here, $\hat{\Pi}_{11} = -\frac{1}{(1+a_1)}$ and $\hat{\Pi}_{12} = -b_1$. We then have

$$F_{b_1}(x, y, z) = \begin{pmatrix} -xy & xy & 0 \end{pmatrix}^T, \; F_{b_1}\left(\hat{E}_1; b_1 = b_1^{TC}\right) = \begin{pmatrix} 0 & 0 & 0 \end{pmatrix}^T \text{ and } V_1^T F_{b_1}\left(\hat{E}_1; b_1 = b_1^{TC}\right) = 0.$$

We also have

$$DF_{b_1}\left(atE_1; b_1 = b_1^{TC}\right)U_1 = (0 \;\; 1 \;\; 0)^T \text{and} V_1^T\left[DF_{b_1}\left(\hat{E}_1; b_1 = b_1^{TC}\right)U_1\right] = 1 \neq 0.$$

Moreover

$$V_1^T D^2F\left(\hat{E}_1; b_1 = b_1^{TC}\right)(U_1, U_1) = \frac{-2\hat{\Pi}_{12}}{\hat{\Pi}_{11}} = -2b_1(1 + a_1) \neq 0.$$

Applying Sotomayor's theorem [32, 33], we conclude that the system undergoes a transcritical bifurcation at $\hat{E}_1$ as b_1 crosses the threshold b_1^{TC}. □

4.3.2. Stability analysis of the system around $\hat{E}_3(\hat{x}_3, \hat{y}_3, \hat{z}_3)$

The Jacobian matrix $J_{\hat{E}_3}$ at $\hat{E}_3$ is given by

$$\begin{bmatrix} \bar{\Pi}_{11} & \bar{\Pi}_{12} & 0 \\ \bar{\Pi}_{21} & 0 & \bar{\Pi}_{23} \\ 0 & \bar{\Pi}_{32} & 0 \end{bmatrix},$$

where $\bar{\Pi}_{11} = \frac{\hat{x}_3\left(-2\hat{x}_3^2+\hat{x}_3+(2-3\hat{x}_3)a_1\right)}{(\hat{f}\hat{y}_3+1)(\hat{x}_3+a_1)^2} - \hat{y}_3 b_1$, $\bar{\Pi}_{12} = \hat{x}_3\left(\frac{\hat{f}(\hat{x}_3-1)\hat{x}_3}{(\hat{f}\hat{y}_3+1)^2(\hat{x}_3+a_1)} - b_1\right)$, $\bar{\Pi}_{21} = \hat{y}_3 b_1 > 0$, $\bar{\Pi}_{23} = -\hat{y}_3 c_1 < 0$, and $\bar{\Pi}_{32} = \hat{z}_3 c_1 > 0$. The characteristic equation of $J_{\hat{E}_3}$ is given by

$$\eta^3 + \hat{A}_1\eta^2 + \hat{A}_2\eta + \hat{A}_3 = 0 \tag{4.25}$$

where the values of A_i are defined as

$$\hat{A}_1 = -\bar{\Pi}_{11},\ \hat{A}_2 = -(\bar{\Pi}_{12}\bar{\Pi}_{21} + \bar{\Pi}_{23}\bar{\Pi}_{32}),\ \hat{A}_3 = \bar{\Pi}_{11}\bar{\Pi}_{23}\bar{\Pi}_{32}.$$

The stability depends on the sign of $\bar{\Pi}_{11}$ and $\bar{\Pi}_{12}$. Let us consider the two cases for $\bar{\Pi}_{11}$. Case 1: If $\bar{\Pi}_{11} > 0$ then $\hat{A}_1 < 0$. Case 2: If $\bar{\Pi}_{11} < 0$ then $\hat{A}_1 > 0$.

If $\bar{\Pi}_{12} < 0$, then $\hat{A}_2$ is always positive since $\bar{\Pi}_{12}\bar{\Pi}_{21} < 0$ and $\bar{\Pi}_{23}\bar{\Pi}_{32} < 0$. Our observation indicates that $\hat{A}_3 > 0$ if $\bar{\Pi}_{11} < 0$. It is easy to check that $\hat{A}_1\hat{A}_2 - \hat{A}_3 = \bar{\Pi}_{11}\bar{\Pi}_{12}\bar{\Pi}_{21} > 0$ if $\bar{\Pi}_{11} < 0$ and $\bar{\Pi}_{12} < 0$.

According to the Routh–Hurwitz criterion, $\hat{E}_3$ is locally asymptotically stable if and only if $\hat{A}_i > 0$, i = 1,2,3 and $\hat{A}_1\hat{A}_2 > \hat{A}_3$.

Proposition 4.2. *The system* (3.2) *experiences a Hopf bifurcation in the vicinity of the coexistence equilibrium $\hat{E}_3$ when the Allee constant reaches the critical value $\hat{f} = \hat{f}_c$, leading to oscillations in the population.*

Proof. The Hopf bifurcation exists at $\hat{f} = \hat{f}_c$ if and only if the following conditions hold:

(i) $\hat{A}_i(\hat{f}_c) > 0$, $i = 1, 2, 3$;
(ii) $\hat{A}_1(\hat{f}_c)\hat{A}_2(\hat{f}_c) - \hat{A}_3(\hat{f}_c) = 0$;
(iii) The eigenvalues of the characteristic equation (4.25) must take the form $\eta_i = u_i + \mathbf{i}v_i$, and $\frac{du_i}{d\hat{f}} \neq 0$, $i = 1, 2, 3$.

To verify the Hopf bifurcation condition (iii), we substitute $\eta = u + \mathbf{i}v$ into the characteristic Eq (4.25), yielding:

$$(u + \mathbf{i}v)^3 + \hat{A}_1(u + \mathbf{i}v)^2 + \hat{A}_2(u + \mathbf{i}v) + \hat{A}_3 = 0. \tag{4.26}$$

By separating the real and imaginary parts and eliminating v, we derive the following equation:

$$8u^3 + 8\hat{A}_1u^2 + 2u(\hat{A}_1^2 + \hat{A}_2) + \hat{A}_1\hat{A}_2 - \hat{A}_3 = 0. \tag{4.27}$$

It is evident that $u(\hat{f}_c) = 0$ if and only if $\hat{A}_1(\hat{f}_c)\hat{A}_2(\hat{f}_c) - \hat{A}_3(\hat{f}_c) = 0$. Moreover, at $\hat{f} = \hat{f}_c$, $u(\hat{f}_c)$ is the only root, as the discriminate $8u^2 + 8\hat{A}_1u + 2(\hat{A}_1^2 + \hat{A}_2) = 0$ if $64\hat{A}_1^2 - 64(\hat{A}_1^2 + \hat{A}_2) < 0$. Differentiating (4.27) with respect to $\hat{f}$, we obtain

$24u^2\frac{du}{d\hat{f}} + 16\hat{A}_1 u\frac{du}{d\hat{f}} + 2(\hat{A}_1^2 + \hat{A}_2)\frac{du}{d\hat{f}} + 2u[2\hat{A}_1\frac{d\hat{A}_1}{d\hat{f}} + \frac{d\hat{A}_2}{d\hat{f}}] + \frac{d\hat{S}}{d\hat{f}} = 0$ where $\hat{S} = \hat{A}_1\hat{A}_2 - \hat{A}_3$. Since at $\hat{f} = \hat{f}_c$, $u(\hat{f}_c) = 0$, we get $\left[\frac{du}{d\hat{f}}\right]_{\hat{f}=\hat{f}_c} = \frac{-\frac{d\hat{S}}{d\hat{f}}}{2(\hat{A}_1^2+\hat{A}_2)} \neq 0$. The expression above confirms that the system undergoes a Hopf bifurcation near the coexistence equilibrium $\hat{E}_3$. □

To analyze the characteristics of the Hopf bifurcation, we consider a perturbation of the system (3.2) in the form: $\dot{\chi} = M\chi + \mathbf{F}(\chi) + O\|\chi\|^4$ where

$\chi = \begin{pmatrix} \bar{X} \\ \bar{Y} \\ \bar{Z} \end{pmatrix}$: $\bar{X} = x - \hat{x}_3, \bar{Y} = y - \hat{y}_3, \bar{Z} = z - \hat{z}_3,$ and $M = J_{\hat{E}_3}$. Here, $\mathbf{F} = \begin{pmatrix} F_1 \\ F_2 \\ F_3 \end{pmatrix}$, where

$$\begin{aligned}
F_1 &= \frac{\left(-a_1^3 - a_1^2\right)}{(a_1+\hat{x}_3)^4(f\hat{y}_3+1)}\bar{X}^3 + \frac{f\left(3a_1\hat{x}_3^2 + 3a_1^2\hat{x}_3 - a_1^2 + \hat{x}_3^3\right)}{(a_1+\hat{x}_3)^3(f\hat{y}_3+1)^2}\bar{X}^2\bar{Y} \\
&+ \frac{f^2\left(-3a_1\hat{x}_3^2 + 2a_1\hat{x}_3 - 2\hat{x}_3^3 + \hat{x}_3^2\right)}{(a_1+\hat{x}_3)^2(f\hat{y}_3+1)^3}\bar{X}\bar{Y}^2 + \frac{f^3(\hat{x}_3-1)\hat{x}_3^2}{(a_1+\hat{x}_3)(f\hat{y}_3+1)^4}\bar{Y}^3 \\
&+ \frac{a_1^2 - 3a_1\hat{x}_3^2 - 3a_1^2\hat{x}_3 - \hat{x}_3^3}{(a_1+\hat{x}_3)^3(f\hat{y}_3+1)}X^2 - \frac{f^2(\hat{x}_3-1)\hat{x}_3^2}{(a_1+\hat{x}_3)(f\hat{y}_3+1)^3}\bar{Y}^2 \\
&- \left(\frac{f\left(-3a_1\hat{x}_3^2 + 2a_1\hat{x}_3 - 2\hat{x}_3^3 + \hat{x}_3^2\right)}{(a_1+\hat{x}_3)^2(f\hat{y}_3+1)^2} + b_1\right)\bar{X}\bar{Y}, \\
F_2 &= b_1\bar{X}\bar{Y} - c_1\bar{Y}\bar{Z}, \\
F_3 &= c_1\bar{Y}\bar{Z}.
\end{aligned}$$

For $i = 1, 2, 3$, $\bar{x} = (\bar{x}_1, \bar{x}_2, \bar{x}_3), \bar{y} = (\bar{y}_1, \bar{y}_2, \bar{y}_3)$, and $\bar{w} = (\bar{w}_1, \bar{w}_2, \bar{w}_3)$, the $B_i(\bar{x}, \bar{y})$ and $C_i(\bar{x}, \bar{y}, \bar{w})$ are of the form

$$\begin{aligned}
B_i(\bar{x}, \bar{y}) &= \sum_{i,j=1, i\leq j}^{3} \left[\frac{\partial^2 F_i}{\partial\zeta_i\partial\zeta_j}(\zeta_1, \zeta_2, \zeta_3)\right]_{(0,0,0)} \bar{x}_i\bar{y}_j, \\
C_i(\bar{x}, \bar{y}, \bar{w}) &= \sum_{i,j,k=1, i\leq j\leq k}^{3} \left[\frac{\partial^3 F_i}{\partial\zeta_i\partial\zeta_j\partial\zeta_3}(\zeta_1, \zeta_2, \zeta_3)\right]_{(0,0,0)} \bar{x}_i\bar{y}_j\bar{w}_k.
\end{aligned}$$

In addition $B(\bar{x}, \bar{y}) = \begin{pmatrix} B_1(\bar{x}, \bar{y}) \\ B_2(\bar{x}, \bar{y}) \\ B_3(\bar{x}, \bar{y}) \end{pmatrix}$ and $C(\bar{x}, \bar{y}, \bar{w}) = \begin{pmatrix} C_1(\bar{x}, \bar{y}, \bar{w}) \\ C_2(\bar{x}, \bar{y}, \bar{w}) \\ C_3(\bar{x}, \bar{y}, \bar{w}) \end{pmatrix}$ are given by

$$\begin{aligned}
B(\bar{x}, \bar{y}) &= \begin{pmatrix} b_{11}x_1y_1 - b_{12}x_1y_2 - b_{22}x_2y_2 \\ b_1\bar{x}_1\bar{y}_2 - c_1\bar{x}_2\bar{y}_3 \\ c_1\bar{x}_2\bar{y}_3 \end{pmatrix} \\
\textit{and } C(\bar{x}, \bar{y}, \bar{w}) &= \begin{pmatrix} -6K\bar{x}_1\bar{y}_1\bar{w}_1 \\ 0 \\ 0 \end{pmatrix}.
\end{aligned}$$

Here, $b_{11} = \frac{\left(-3a_1\hat{x}_3^2-3a_1^2\hat{x}_3+a_1^2-\hat{x}_3^3\right)}{(a_1+\hat{x}_3)^3(f\hat{y}_3+1)}$, $b_{12} = \left(\frac{f\left(-3a_1\hat{x}_3^2+2a_1\hat{x}_3-2\hat{x}_3^3+\hat{x}_3^2\right)}{(a_1+\hat{x}_3)^2(f\hat{y}_3+1)^2} + b_1\right)$, and $b_{22} = \frac{\left(f^2(\hat{x}_3-1)\hat{x}_3^2\right)}{(a_1+\hat{x}_3)(f\hat{y}_3+1)^3}$. Moreover, $F(\chi) = \frac{1}{2}B(\chi,\chi) + \frac{1}{2}C(\chi,\chi,\chi)$.

The normalized eigenvector corresponding to the eigenvalue $i\omega$ of the matrix M and $-i\omega$ of the matrix M^T are given by

$$q = \begin{pmatrix} q_1 \\ q_2 \\ q_3 \end{pmatrix} = \frac{1}{|q|}\begin{pmatrix} -\frac{\Pi_{12}(\Pi_{11}+i\omega)}{\Pi_{11}^2+\omega^2} \\ 1 \\ -\frac{i\Pi_{32}}{\omega} \end{pmatrix} \text{ and } p = \begin{pmatrix} p_1 \\ p_2 \\ p_3 \end{pmatrix} = \frac{1}{|p|}\begin{pmatrix} -\frac{\Pi_{21}(\Pi_{11}-i\omega)}{\Pi_{11}^2+\omega^2} \\ 1 \\ \frac{i\Pi_{23}}{\omega} \end{pmatrix}$$

respectively.

Here, $M^{-1} = \begin{pmatrix} \frac{1}{\Pi_{11}} & 0 & -\frac{\Pi_{12}}{\Pi_{11}\Pi_{32}} \\ 0 & 0 & \frac{1}{\Pi_{32}} \\ -\frac{\Pi_{21}}{\Pi_{11}\Pi_{23}} & \frac{1}{\Pi_{23}} & \frac{\Pi_{12}\Pi_{21}}{\Pi_{11}\Pi_{23}\Pi_{32}} \end{pmatrix}$, and

$$M^{-1}B(q,\bar{q}) =) = \begin{pmatrix} s_1 \\ s_2 \\ s_3 \end{pmatrix} = \begin{pmatrix} \frac{1}{\Pi_{11}}S_1 - \frac{\Pi_{12}}{\Pi_{11}}\frac{ic_1}{\omega} \\ \frac{ic_1}{\omega} \\ -\frac{\Pi_{21}}{\Pi_{11}\Pi_{23}}S_1 - \frac{1}{\Pi_{23}}\left(\frac{b_1\Pi_{12}(\Pi_{11}+i\omega)}{\Pi_{11}^2+\omega^2} + \frac{ic_1\Pi_{32}}{\omega}\right) + \frac{\Pi_{12}\Pi_{21}}{\Pi_{11}\Pi_{23}}\frac{ic_1}{\omega} \end{pmatrix}, \text{ where}$$

$$S_1 = b_{11}\frac{\Pi_{12}^2}{\Pi_{11}^2+\omega^2} + b_{12}\frac{\Pi_{12}(\Pi_{11}+i\omega)}{\Pi_{11}^2+\omega^2} - b_{22}.$$

Note that

$$\begin{aligned} & (2i\omega I_3 - M)^{-1} \\ = \; & \frac{1}{|2i\omega I_3 - M|}\begin{pmatrix} 4\mathrm{i}\omega^2 - \Pi_{23}\Pi_{32} & 2\mathrm{i}\omega\Pi_{12} & \Pi_{12}\Pi_{23} \\ 2\mathrm{i}\omega\Pi_{21} & 4\mathrm{i}\omega^2 - 2\mathrm{i}\omega\Pi_{11} & 2\mathrm{i}\omega\Pi_{23} - \Pi_{11}\Pi_{23} \\ \Pi_{21}\Pi_{32} & 2\mathrm{i}\omega\Pi_{32} - \Pi_{11}\Pi_{32} & E \end{pmatrix} \end{aligned}$$

where $E = (2\mathrm{i}\omega - \Pi_{11})\,2\mathrm{i}\omega - \Pi_{12}\Pi_{21}$, and $|2i\omega I_3 - M| = -4\Pi_{11}\mathrm{i}\omega^2 - 2\Pi_{12}\Pi_{21}\mathrm{i}\omega - 2\Pi_{23}\Pi_{32}\mathrm{i}\omega + \Pi_{11}\Pi_{23}\Pi_{32} + 8\mathrm{i}\omega^3$.

We now get

$$\begin{aligned} & (2i\omega I_3 - M)^{-1}B(q,q) \\ = \; & (2i\omega I_3 - M)^{-1}\begin{pmatrix} b_{11}q_1^2 - b_{12}q_1q_2 - b_{22}q_2^2 \\ b_1q_1q_2 - c_1q_2q_3 \\ c_1q_2q_3 \end{pmatrix} \\ = \; & \frac{1}{|2i\omega I_3 - M|}\begin{pmatrix} \left(4\mathrm{i}\omega^2 - \Pi_{23}\Pi_{32}\right)\tau_1 + 2\mathrm{i}\omega\Pi_{12}\tau_2 + \Pi_{12}\Pi_{23}\tau_3 \\ 2\mathrm{i}\omega\Pi_{21}\tau_1 + \left(4\mathrm{i}\omega^2 - 2\mathrm{i}\omega\Pi_{11}\right)\tau_2 + (2\mathrm{i}\omega\Pi_{23} - \Pi_{11}\Pi_{23})\,\tau_3 \\ \Pi_{21}\Pi_{32}\tau_1 + (2\mathrm{i}\omega\Pi_{32} - \Pi_{11}\Pi_{32})\,\tau_2 + E\tau_3 \end{pmatrix} \end{aligned}$$

where

$$\tau_1 \;=\; b_{11}q_1^2 - b_{12}q_1q_2 - b_{22}q_2^2,\; \tau_2 = b_1q_1q_2 - c_1q_2q_3,\; \tau_3 = c_1q_2q_3.$$

The first Lyapunov coefficient $l_1(0)$ ([34]) is calculated as: $l_1(0)$ $= \frac{1}{2\omega}Re[< \mathrm{p}, \mathrm{c}(\mathrm{q},\mathrm{q},\bar{\mathrm{q}}) > -2 < \mathrm{p}, B(\mathrm{q}, M^{-1}B(\mathrm{q},\bar{\mathrm{q}})) > + < \mathrm{p}, B(\bar{\mathrm{q}}, (2\mathrm{i}\omega I - M)^{-1}B(\mathrm{q},\mathrm{q})) >]$. If $l_1(0) < 0$, the Hopf bifurcation is supercritical, which implies that the resulting limit cycles are stable.

Remark 2. *Bifurcation analysis reveals critical thresholds where small changes in the ecological parameters lead to qualitative shifts in the system's dynamics. Each equilibrium point corresponds to a specific ecological state: Extinction (E_0), prey-only survival (E_1), super-predator-free (E_2), and full food chain persistence (E_3). Transcritical and Hopf bifurcations at these points mark transitions such as predator invasion, oscillatory dynamics, or loss of stability due to the Allee effect and fear effect.*

Analyzing boundary equilibria like E_2 is essential, as they represent intermediate ecological scenarios (e.g., absence of the top predator). Bifurcations at E_2 indicate conditions for species' persistence or extinction, offering insights into trophic cascades and recovery potential. Thus, discussing all equilibrium points, including boundary cases, is crucial for a complete understanding of the system's ecological dynamics.

5. Spatially explicit model system

This section integrates the spatial aspect of ecological interactions into the temporal system (3.2) by transforming the ODE system into a PDE system through the use of reaction-diffusion equations. The size of the prey, predator, and the main predator population at any location $(U, V) \in \Omega$ and time t, is given by $x(t, U, V)$, $y(t, U, V)$, and $z(t, U, V)$, respectively, where $\Omega \subset \mathbb{R}^2$ is a bounded domain with a smooth boundary $\partial\Omega$. The spatiotemporal model [35] associated with the temporal model (3.2) is represented by the subsequent reaction-diffusion system:

$$\begin{aligned}
\frac{\partial x}{\partial \tau} &= \frac{x}{1+\hat{f}y}(1-x)\frac{x}{x+a_1} - b_1xy + d_1\Delta x,\\
\frac{\partial y}{\partial \tau} &= b_1xy - c_1yz - \hat{d}_1y + d_2\Delta y,\\
\frac{\partial z}{\partial \tau} &= c_1yz - \hat{d}_2z + d_3\Delta z,
\end{aligned} \tag{5.1}$$

subjected to non-negative initial conditions and the zero-flux boundary conditions

$$\begin{aligned}
&x(0, U, V) \geq 0, \quad y(0, U, V) \geq 0, \quad z(0, U, V) \geq 0 \quad (U, V) \in \Omega,\\
&\frac{\partial x}{\partial \nu} = \frac{\partial y}{\partial \nu} = \frac{\partial z}{\partial \nu} = 0, \quad (U, V) \in \partial\Omega, \quad t > 0,
\end{aligned} \tag{5.2}$$

where d_1, d_2, and d_3 are self-diffusion coefficients of the prey, predator, and top–predator, respectively; ν is the outward unit normal to $\partial\Omega$; and the Laplace operator $\Delta = \frac{\partial^2}{\partial U^2} + \frac{\partial^2}{\partial V^2}$. Only the self-diffusion terms have been addressed in the model formulation (5.1) above. The presence, absence, abundance, and scarcity of the predator population, and vice versa, have a significant impact on the movement of prey individuals in a realistic ecological framework. This is referred to as cross-diffusion [36–39], and it is not reducible to self-diffusion terms alone in a spatiotemporal predator-prey model. Cross-diffusion and self-diffusion in the predator-prey paradigm with the "fear effect" have been examined in

very few studies. After adding the cross-diffusion terms, the system (5.1) now looks like this:

$$\begin{aligned}
\frac{\partial x}{\partial \tau} &= \frac{x}{1+\hat{f}y}(1-x)\frac{x}{x+a_1} - b_1xy + \Delta(d_1x + d_{12}xy),\\
\frac{\partial y}{\partial \tau} &= b_1xy - c_1yz - \hat{d}_1y + \Delta(d_2y + d_{21}xy),\\
\frac{\partial z}{\partial \tau} &= c_1yz - \hat{d}_2z + d_3\Delta z,
\end{aligned} \tag{5.3}$$

where the cross-diffusion coefficients of the prey and predator populations are denoted by d_{12} and d_{21}, respectively. Since d_{12} and d_{21} are assumed to be positive constants, $d_{12} > 0$ indicates that prey is migrating toward areas with fewer predators, and $d_{21} > 0$ indicates that predator species prefer to hunt prey from lower groups of the prey population in order to evade larger groups' group defense. Our initial and boundary conditions are the same as those provided in Eq (5.2).

5.1. Stability analysis of the spatial model system

In the context of ecological systems, complex patterns such as "leaser slime" formations in slime moulds are of particular interest. These patterns emerge from the collective behavior of individual organisms responding to environmental cues and resource availability. The study of such patterns provides insights into nutrient cycling and microbial interactions, and serves as indicators of an ecosystem's health and biodiversity.

To discuss the linear stability analysis of the model system (5.3) for the spatially homogeneous steady state $E^*(x^*, y^*, z^*)$ and to explore the possible "leaser slime" patterns [40–42], we linearize [36] this system using the transformations

$$\begin{aligned}
x(\tau, U, V) &= x^* + \hat{x}(\tau, U, V),\\
y(\tau, U, V) &= y^* + \hat{y}(\tau, U, V),\\
z(\tau, U, V) &= z^* + \hat{z}(\tau, U, V),
\end{aligned} \tag{5.4}$$

where $\hat{x}(\tau, U, V)$, $\hat{y}(\tau, U, V)$, and $\hat{z}(\tau, U, V)$ are small time and space perturbations. Conventionally, $\hat{x}$, $\hat{y}$, and $\hat{z}$, are taken as

$$\begin{aligned}
\hat{x}(\tau, U, V) &= \epsilon_1 \exp\left(\lambda_K\tau + i(K_UU + K_VV)\right),\\
\hat{y}(\tau, U, V) &= \epsilon_2 \exp\left(\lambda_K\tau + i(K_UU + K_VV)\right),\\
\hat{z}(\tau, U, V) &= \epsilon_3 \exp\left(\lambda_K\tau + i(K_UU + K_VV)\right),
\end{aligned} \tag{5.5}$$

where $0 < \epsilon_1,\ \epsilon_2,\ \epsilon_3 \ll 1$, and λ_K is the wavelength. In addition, $\mathbb{K} = (K_U, K_V)$ is the wave number vector and $K = |\mathbb{K}|$ is the wave number.

Substituting (5.4) and (5.5) in the spatial system (5.3), we have

$$\begin{aligned}
\frac{\partial \hat{x}}{\partial \tau} &= m_{11}\hat{x} + m_{12}\hat{y} + m_{13}\hat{z} - K^2(d_1 + d_{12}y^*)\hat{x} - K^2(d_{12}x^*)\hat{y},\\
\frac{\partial \hat{y}}{\partial \tau} &= m_{21}\hat{x} + m_{22}\hat{y} + m_{23}\hat{z} - K^2(d_{21}y^*)\hat{x} - K^2(d_2 + d_{21}x^*)\hat{y},\\
\frac{\partial \hat{y}}{\partial \tau} &= m_{31}\hat{x} + m_{32}\hat{y} + m_{33}\hat{z} - K^2d_3\hat{z},
\end{aligned} \tag{5.6}$$

where
$m_{11} = -b_1y^* + \frac{x^*(a_1(2-3x^*)+x^*-2x^{*2})}{(a_1+x^*)^2(1+\hat{f}y^*)}$, $m_{12} = -b_1x^* + \frac{\hat{f}(-1+x^*)x^{*2}}{(a_1+x^*)(1+\hat{f}y^*)^2}$, $m_{13} = 0$,
$m_{21} = b_1y^*$, $m_{22} = 0$, $m_{23} = -c_1y^*$,
$m_{31} = 0$, $m_{32} = c_1z^*$, $m_{33} = 0$.

The characteristic equation of the linearized system (5.6) is given by

$$\det(J_K - \lambda I_3) = 0, \tag{5.7}$$

where

$$J_K = \begin{pmatrix} m_{11} - (d_1 + d_{12}y^*)K^2 & m_{12} - d_{12}x^*K^2 & 0 \\ m_{21} - d_{21}y^*K^2 & -(d_2 + d_{21}x^*)K^2 & m_{23} \\ 0 & m_{32} & -d_3K^2 \end{pmatrix}.$$

In simplified form, the characteristic Eq (5.7) can be rewritten as

$$\lambda^3 + \mu_2(K^2)\lambda^2 + \mu_1(K^2)\lambda + \mu_0(K^2) = 0, \tag{5.8}$$

where

$$\begin{aligned}
\mu_2(K^2) &= -m_{11} + K^2(d_1 + d_{12}y^* + d_2 + d_{21}x^* + d_3), \\
\mu_1(K^2) &= -m_{12}m_{21} - m_{23}m_{32} \\
&\quad + K^2(-m_{11}(d_2 + d_3 + d_{21}x^*) + m_{21}d_{12}x^* + m_{12}d_{21}y^*) \\
&\quad + K^4\Big(d_1(d_2 + d_3 + d_{21}x^*) + d_2(d_3 + d_{12}y^*) + d_3(d_{21}x^* + d_{12}y^*)\Big), \\
\mu_0(K^2) &= K^6(d_1d_2d_3 + d_1d_{21}d_3x^* + d_{12}d_2d_3y^*) \\
&\quad + K^4\Big(-d_2d_3m_{11} + d_3(-d_{21}m_{11} + d_{12}m_{21})x^* + d_{21}d_3m_{12}y^*\Big) \\
&\quad + K^2\Big(-d_3m_{12}m_{21} - d_1m_{23}m_{32} - d_{12}m_{23}m_{32}y^*\Big) + m_{11}m_{23}m_{32}.
\end{aligned}$$

These coefficients, in simplified form, can be written as

$$\begin{aligned}
\mu_2(K^2) &= (d_1 + d_{12}y^* + d_2 + d_{21}x^* + d_3)K^2 + A_1, \\
\mu_1(K^2) &= A_2 + \Big(-m_{11}(d_2 + d_3 + d_{21}x^*) + m_{21}d_{12}x^* + m_{12}d_{21}y^*\Big)K^2 \\
&\quad + \Big(d_1(d_2 + d_3 + d_{21}x^*) + d_2(d_3 + d_{12}y^*) + d_3(d_{21}x^* + d_{12}y^*)\Big)K^4, \\
\mu_0(K^2) &= \Big(d_1d_2d_3 + d_1d_{21}d_3x^* + d_{12}d_2d_3y^*\Big)K^6 \\
&\quad + \Big(-d_2d_3m_{11} + d_3(-d_{21}m_{11} + d_{12}m_{21})x^* + d_{21}d_3m_{12}y^*\Big)K^4 \\
&\quad + \Big(-d_3m_{12}m_{21} - d_1m_{23}m_{32} - d_{12}m_{23}m_{32}y^*\Big)K^2 + A_3, \\
[\mu_2\mu_1 - \mu_0](K^2) &\\
&= \Big(d_1 + d_2 + d_{21}x^* + d_{12}y^*\Big)\Big[(d_1 + d_3)(d_2 + d_3 + d_{21}x^*)
\end{aligned}$$

$$
\begin{aligned}
&+ d_{12}(d_2 + d_3)y^*\Big]K^6 + \\
&\Big[d_2d_3m_{11} + d_3(d_{21}m_{11} - d_{12}m_{21})x^* - d_{21}d_3m_{12}y^* \\
&+ A_1(d_3(d_2 + d_{21}x^*) + d_1(d_2 + d_3 + d_{21}x^*) + d_{12}(d_2 + d_3)y^*) \\
&- (d_1 + d_2 + d_3 + d_{21}x^* + d_{12}y^*) \\
&\quad \times (d_2m_{11} + d_3m_{11} + d_{21}m_{11}x^* - d_{12}m_{21}x^* - d_{21}m_{12}y^*)\Big]K^4 \\
&+ \Big[d_3m_{12}m_{21} + m_{23}m_{32}(d_1 + d_{12}y^*) \\
&+ A_2(d_1 + d_2 + d_3 + d_{21}x^* + d_{12}y^*) \\
&- A_1(d_2m_{11} + d_3m_{11} + d_{21}m_{11}x^* - d_{12}m_{21}x^* - d_{21}m_{12}y^*)\Big]K^2 \\
&+ A_1A_2 - A_3.
\end{aligned}
$$

where $A_1 = -m_{11}$, $A_2 = -m_{12}m_{21} - m_{23}m_{32}$, and $A_3 = m_{11}m_{23}m_{32}$.

According to the Routh–Hurwitz criterion for stability, $\mathrm{Re}(\lambda) < 0$ in the model system (5.3) around the equilibrium point $E_3(x^*, y^*, z^*)$ if and only if the following conditions hold:

$$\mu_2(K^2) > 0, \quad \mu_1(K^2) > 0, \quad \mu_0(K^2) > 0, \quad \text{and} \quad [\mu_2\mu_1 - \mu_0](K^2) > 0. \tag{5.9}$$

Theorem 4. *Suppose that the interior equilibrium point $E_3(x^*, y^*, z^*)$ is Locally Asymptotically Stable (LAS) for the temporal system. Then $E_3(x^*, y^*, z^*)$ is LAS for the spatiotemporal system* (5.3) *if the condition* (5.9) *holds.*

5.2. Cross-diffusion-driven Turing instability

Cross-diffusion-induced diffusion-driven instability on stationary domains occurs when a homogeneous steady state $E_3(x^*, y^*, z^*)$ is linearly stable in the absence of cross- and regular diffusion, and becomes unstable when cross- and regular diffusion are present [36, 43]. That is

$$\mathrm{Re}(\lambda(K^2 \neq 0)) > 0, \quad \text{for some} \quad K \neq 0 \quad \text{and} \quad \mathrm{Re}(\lambda(K^2 = 0)) < 0. \tag{5.10}$$

Therefore, for Turing instability to occur in the spatial system (5.3), it is necessary that the condition (5.9) fails to exist. Here, $\mu_2(K^2) > 0$, and $\mu_0(K^2) > 0$, for all $K \neq 0$, as the diffusion coefficients are positive and $m_{11} < 0$ and $m_{12} < 0$ from the stability of the homogeneous steady state $E_3(x^*, y^*, z^*)$. Thus, for diffusive instability, we require that $\mu_1(K^2) < 0$, or $[\mu_2\mu_1 - \mu_0](K^2) < 0$ for some $K \neq 0$, where

$$
\begin{aligned}
\mu_1(K^2) &= A_2 + (-m_{11}(d_2 + d_3 + d_{21}x^*) + m_{21}d_{12}x^* + m_{12}d_{21}y^*)K^2 \\
&\quad + (d_1(d_2 + d_3 + d_{21}x^*) + d_2(d_3 + d_{12}y^*) + d_3(d_{21}x^* + d_{12}y^*))K^4, \\
[\mu_2\mu_1 - \mu_0](K^2) &= q_1K^6 + q_2K^4 + q_3K^2 + A_1A_2 - A_3,
\end{aligned} \tag{5.11}
$$

$$
\begin{aligned}
q_1 =& (d_1 + d_2 + d_{21}x^* + d_{12}y^*)((d_1 + d_3)(d_2 + d_3 + d_{21}x^*) + d_{12}(d_2 + d_3)y^*), \\
q_2 =& d_2d_3m_{11} + d_3(d_{21}m_{11} - d_{12}m_{21})x^* - d_{21}d_3m_{12}y^* + A_1(d_3(d_2 + d_{21}x^*) \\
&+ d_1(d_2 + d_3 + d_{21}x^*) + d_{12}(d_2 + d_3)y^*) - (d_1 + d_2 + d_3 + d_{21}x^* + d_{12}y^*) \\
&\times (d_2m_{11} + d_3m_{11} + d_{21}m_{11}x^* - d_{12}m_{21}x^* - d_{21}m_{12}y^*), \\
q_3 =& d_3m_{12}m_{21} + m_{23}m_{32}(d_1 + d_{12}y^*) + A_2(d_1 + d_2 + d_3 + d_{21}x^* + d_{12}y^*) \\
&- A_1(d_2m_{11} + d_3m_{11} + d_{21}m_{11}x^* - d_{12}m_{21}x^* - d_{21}m_{12}y^*).
\end{aligned} \tag{5.12}
$$

Theorem 5. *Suppose that* $b_1y^* > \frac{x^*(a_1(2-3x^*)+x^*-2x^{*2})}{(a_1+x^*)^2(1+\hat{f}y^*)}$ *and* $b_1x^* > \frac{\hat{f}(-1+x^*)x^{*2}}{(a_1+x^*)(1+\hat{f}y^*)^2}$, *in which case, the Turing instability occurs in the system* (5.3) *around* $E_3(x^*, y^*, z^*)$, *provided that any of the following conditions hold:*

(i) $A_2 + (-m_{11}(d_2 + d_3 + d_{21}x^*) + m_{21}d_{12}x^* + m_{12}d_{21}y^*)K^2 + (d_1(d_2 + d_3 + d_{21}x^*) + d_2(d_3 + d_{12}y^*) + d_3(d_{21}x^* + d_{12}y^*))K^4 < 0$ *for some* $K \neq 0$.

(ii) $(d_1+d_2+d_{21}x^*+d_{12}y^*)((d_1+d_3)(d_2+d_3+d_{21}x^*)+d_{12}(d_2+d_3)y^*)K^6+(d_2d_3m_{11}+d_3(d_{21}m_{11}-d_{12}m_{21})x^*-d_{21}d_3m_{12}y^*+A_1(d_3(d_2+d_{21}x^*)+d_1(d_2+d_3+d_{21}x^*)+d_{12}(d_2+d_3)y^*)-(d_1+d_2+d_3+d_{21}x^*+d_{12}y^*)\times(d_2m_{11}+d_3m_{11}+d_{21}m_{11}x^*-d_{12}m_{21}x^*-d_{21}m_{12}y^*))K^4+(d_3m_{12}m_{21}+m_{23}m_{32}(d_1+d_{12}y^*)+A_2(d_1+d_2+d_3+d_{21}x^*+d_{12}y^*)-A_1(d_2m_{11}+d_3m_{11}+d_{21}m_{11}x^*-d_{12}m_{21}x^*-d_{21}m_{12}y^*)K^2+A_1A_2-A_3<0$, *for some* $K \neq 0$.

Example 1. *In this example, we have explored the phenomenon numerically. The parameter values are taken as*

$$\begin{aligned} &a_1 = 0.1,\ b_1 = 0.5,\ c = 0.1,\ \hat{d}_1 = 0.1,\ \hat{d}_2 = 0.1,\ \hat{f} = 0.01,\\ &d_1 = 0.02,\ d_2 = 0.05,\ d_3 = 0.01,\ \ d_{12} = 0.15,\ \ d_{21} = 2. \end{aligned} \tag{5.13}$$

For this set of parameter values $A_1 = 0.15986 > 0$, $A_2 = 0.09623 > 0$, $A_3 = 0.00121 > 0$, *and* $A_1A_2 - A_3 = 0.014175 > 0$; *therefore the temporal system* (3.2) *is stable. We show the* $\mu_2(K^2)$ *vs. K plot,* $\mu_1(K^2)$ *vs. K plot,* $\mu_0(K^2)$ *vs. K plot, and* $[\mu_2\mu_1 - \mu_0](K^2)$ *vs. K plot in Figure 2. Here,* $\mu_1(K^2) < 0$ *for some range of values of K (cf. Figure 2(b)); similarly,* $[\mu_2\mu_1 - \mu_0](K^2) < 0$ *for some range of values of K (cf. Figure 2(d)). This implies that the homogeneous steady state* $E^*(0.35121, 1, 0.75606)$ *becomes unstable for small perturbations, leading to Turing instability (diffusion-driven instability).*

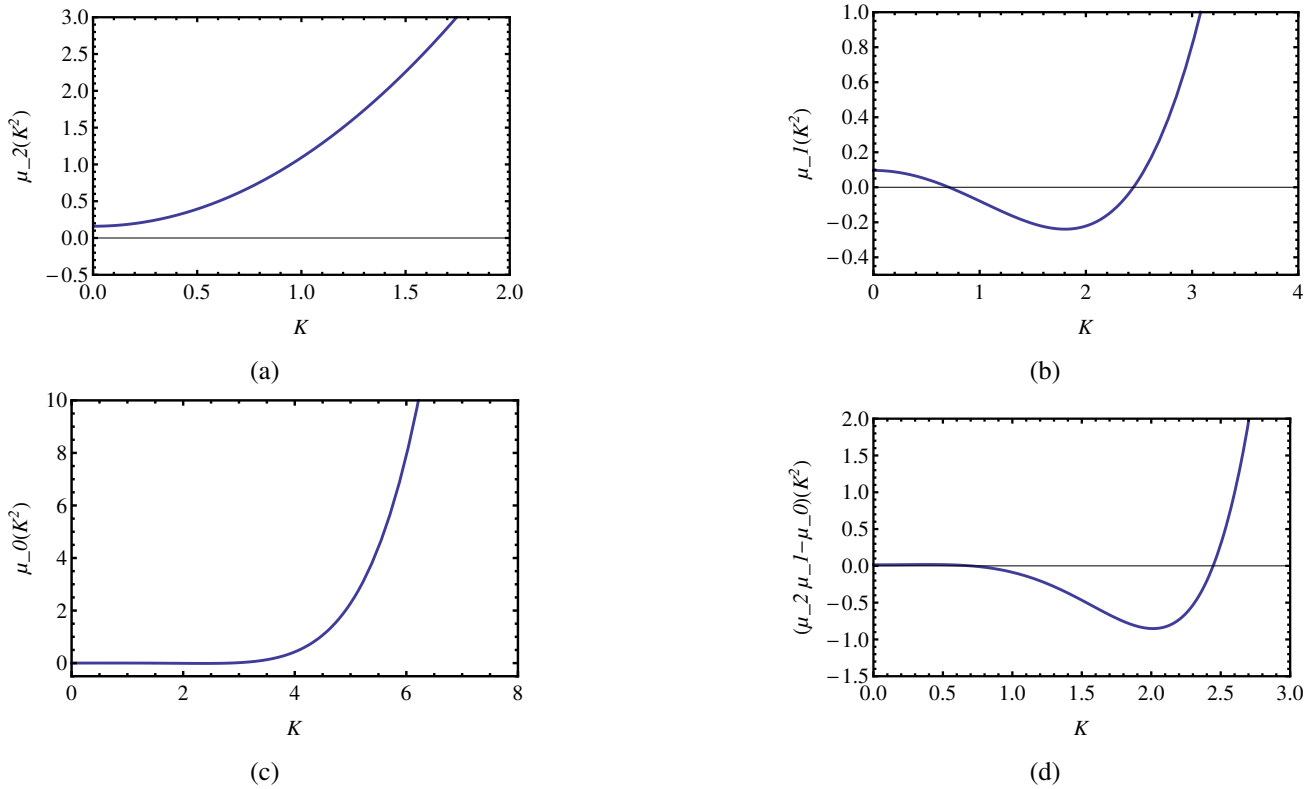

Figure 2. Plot showing the occurrence of Turing instability (diffusion-driven instability).

Example 2. *In our spatial model system* (5.3)*, we have incorporated cross-diffusion and the species' self-diffusion. In Figure 3(a), we illustrate the effect of the cross-diffusion coefficient* d_{12} *on the Turing instability. For this, we have taken the parameters as given in Eq* (5.13)*, except the cross-diffusion* d_{12} *of the prey due to predator. At* $d_{12} = 0.02$, $[\mu_2\mu_1 - \mu_0](K^2) < 0$ *for some values of* $K \neq 0$ *i.e., the system remains unstable. Increasing the value of* d_{12} *to* 0.15 *and* 10*, it is observed that at* $d_{12} = 10$, $[\mu_2\mu_1 - \mu_0](K^2) > 0$ *for all K; i.e., the system becomes stable (cf. Figure 3(a)). Thus, by increasing the cross-diffusion coefficient* d_{12}*, diffusion-induced instabilities shift to stable dynamics. Thus, cross-diffusion of the prey species* d_{12} *stabilizes the spatial dynamics of the system* (5.3).

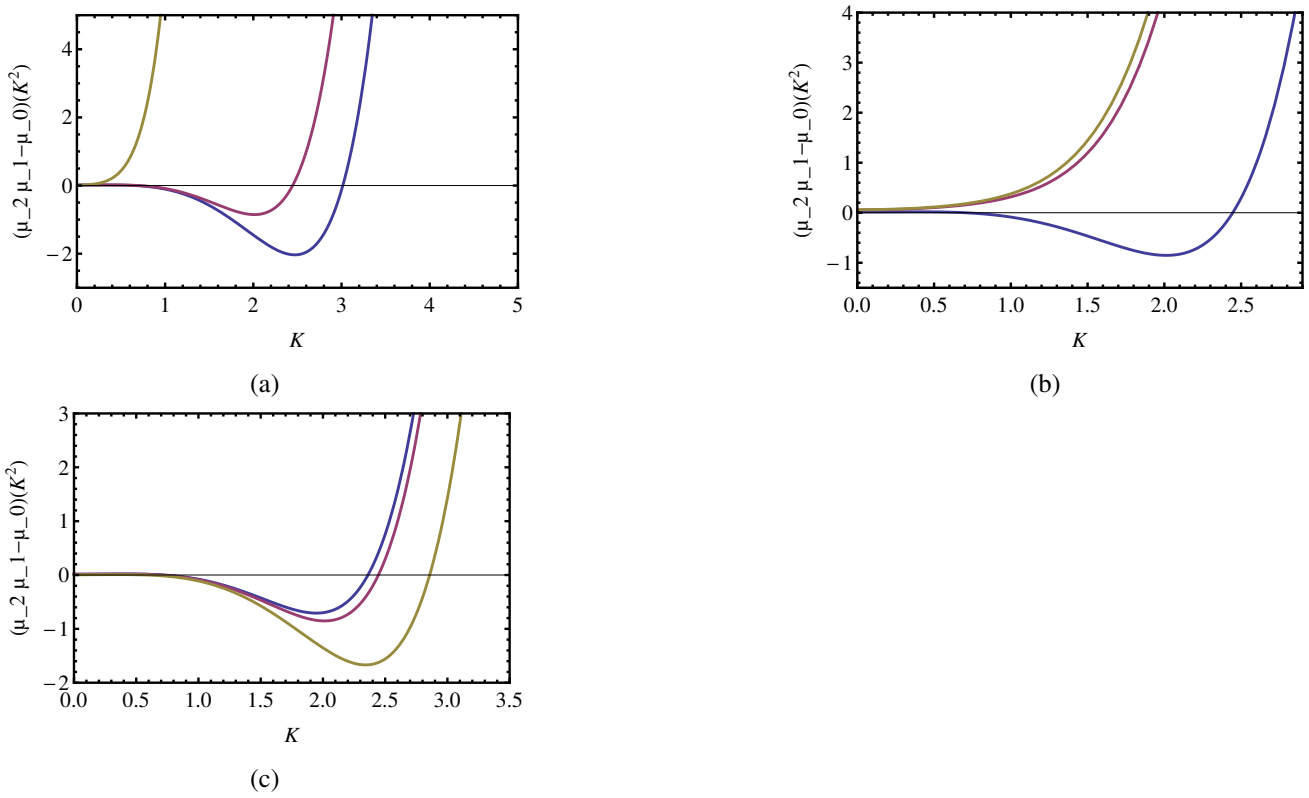

Figure 3. (a) Graph of $[\mu_2\mu_1 - \mu_0](K^2)$ vs. K for different values of the cross-diffusion coefficient $d_{12} = 0.02$ (blue), $d_{12} = 0.15$ (purple), and $d_{12} = 10$ (brown). (b) Graph of $[\mu_2\mu_1 - \mu_0](K^2)$ vs. K for different values of $a_1 = 0.001$ (brown), $a_1 = 0.01$ (purple), and $a_1 = 0.1$ (blue). (c) Graph of $[\mu_2\mu_1 - \mu_0](K^2)$ vs. K for different values of the fear level $k = 0.001$ (blue), $k = 0.01$ (purple), and $k = 0.06$ (brown).

Again, we have plotted $[\mu_2\mu_1 - \mu_0](K^2)$ *vs. K plots for three different values of parameter* $a_1 = \frac{n}{k}$*, where n is the Allee effect constant (cf. Figure 3(b)); the remaining parameter values are the same as those given in Eq* (5.13)*. Initially at* $a_1 = 0.001$, $[\mu_2\mu_1 - \mu_0](K^2) > 0$ *for all values of K, i.e., the system* (5.3) *is stable. Increasing the value of* a_1 *to* 0.01 *and* 0.1*, it is observed that at* 0.1, $[\mu_2\mu_1 - \mu_0](K^2) < 0$ *for some values of K, (cf. Figure 3(b)) i.e., the system is unstable. This implies that the stable dynamics of the system* (5.3) *become unstable with an increase in the value of* a_1*. Therefore,* a_1 *destabilizes the spatial dynamics of the system* (5.3).

Again, we have plotted $[\mu_2\mu_1 - \mu_0](K^2)$ *vs. K plots for three different values of the fear level k (cf.*

Figure 3(c)); the remaining parameter values are same as the given in Eq (5.13). *It is observed that for all the feasible values of the fear level* $k = 0.001,\ 0.01$, *and 0.06,* $[\mu_2\mu_1 - \mu_0](K^2) < 0$ *for some values of K (cf. Figure 3(c)), i.e., the system remains unstable. This implies that the fear level does not significantly impact the spatial dynamics of the system* (5.3).

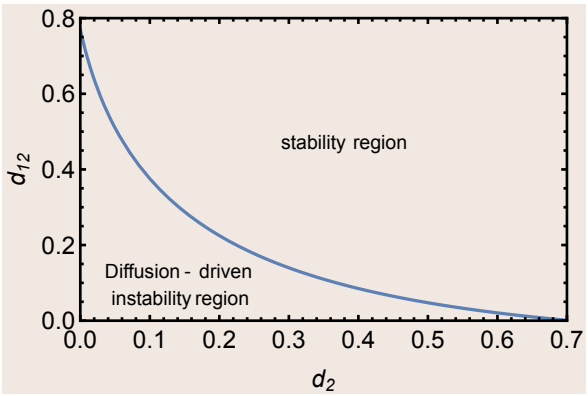

(a)

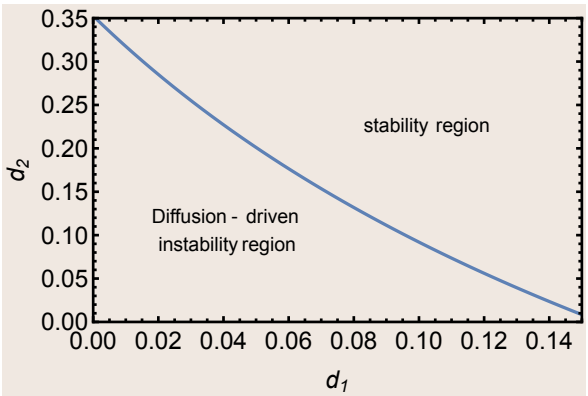

(b)

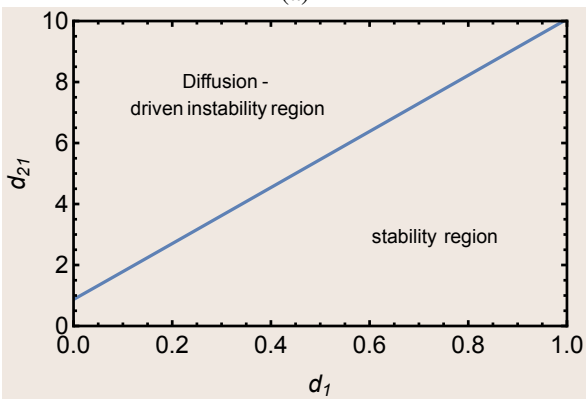

(c)

Figure 4. (a) Turing bifurcation curve for the system (5.3) taking $d_{12} > 0$, $d_2 > 0$, $d_1 = 0.02$, and $d_{21} = 2$; the other parameter values are given in (5.13). (b) Turing bifurcation curve for the system (5.3) taking $d_1 > 0$, $d_2 > 0$, $d_{12} = 0.15$, $d_{21} = 2$, with the other parameter values given in (5.13). (c) Turing bifurcation curve for the system (5.3) taking $d_1 > 0$, $d_{21} > 0$, $d_{12} = 0.15$, and $d_2 = 0.05$, with the other parameter values given in (5.13).

To provide graphical representations of the diffusion-driven instability regions for Turing patterns, we have plotted the Turing bifurcation curve in the $d_2 - d_{12}$ plane (cf. Figure 4(a)), in $d_1 - d_2$ plane (cf. Figure 4(b)), and in $d_1 - d_{21}$ plane (cf. Figure 4(c)); the other parameter values are the same as given in Eq (5.13). In the figures (cf. Figure 4(a),(b)), the blue line denotes the Turing bifurcation curve, and the regions below and above the line are the diffusion-driven instability region and the stability regions, respectively. In Figure 4(c), the blue line denotes the Turing bifurcation curve, and the regions above and below the line are the diffusion-driven instability region and the stability regions, respectively.

6. Numerical simulations

In this section, we present a series of numerical simulations to better understand the system's dynamics and to support the analytical findings. Simulation experiments were carried out in MATLAB (R2013a) and MATCONT (a toolbox of MATLAB, which is mainly used for bifurcation analyses of the linear and nonlinear systems of ordinary differential equations) using the fourth-order Runge-Kutta method. Wolfram Mathematica 9 software was used for the analytical computations. All these simulation experiments were carried out on a laptop with a Windows 10 (64-bit) operating system and an Intel Core i5 (8th Gen) processor.

6.1. Allee effect without fear

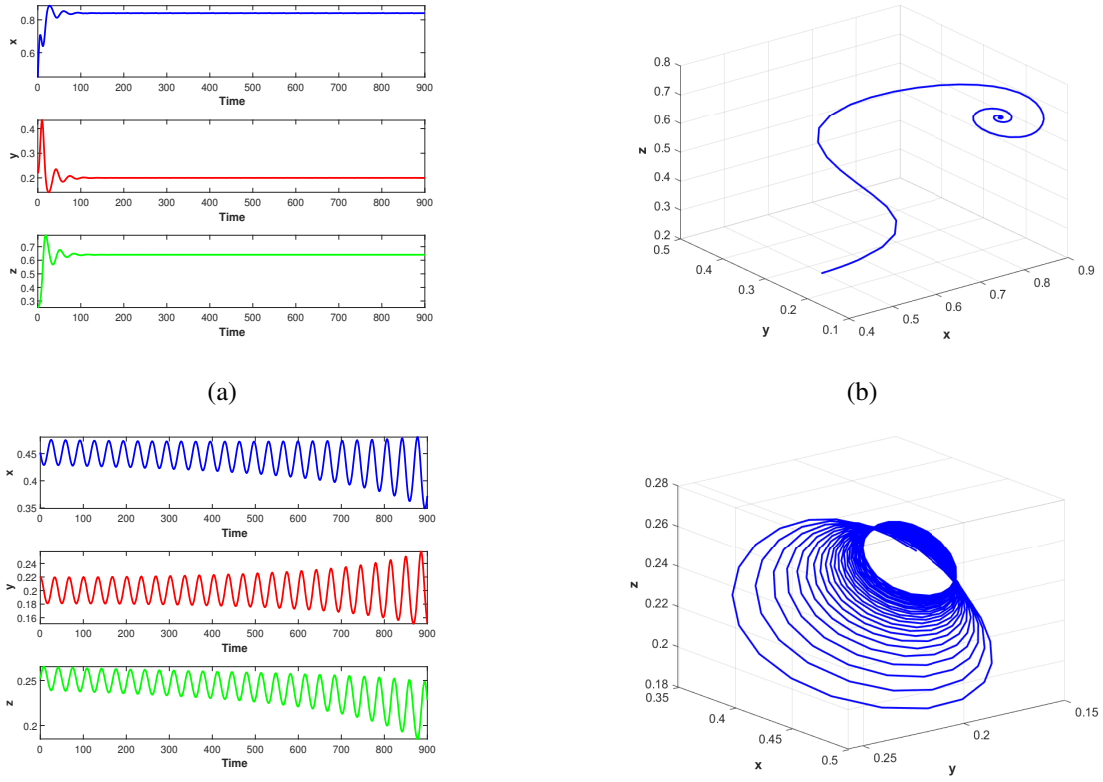

Figure 5. Panels (a) and (b) show, respectively, the time-series of the three species and the phase-plane portrait around the coexistence equilibrium E_3 for $a_1 = 0.5$, $b_1 = 0.5$, $c_1 = 0.5$, $\hat{d}_1 = 0.1$, and $\hat{d}_2 = 0.1$ with the initial condition $[x(0), y(0), z(0)] = [0.452, 0.22, 0.252]$. Panels (c) and (d) display the analogous time-series and phase portrait when a Hopf bifurcation occurs at E_3, with the same parameter values except $a_1 = 2.025$ (all other parameters and the initial condition unchanged).

With the parameter values $a_1 = 0.5$, $b_1 = 0.5$, $c_1 = 0.5$, $\hat{d}_1 = 0.1$, and $\hat{d}_2 = 0.1$ [30], we present the phase trajectory diagram of the dynamic system and a species-time 2D plot. Figure 5(a),(b) illustrates

the populations of x, y, and z approaching their equilibrium values E_3. To quantitatively investigate the impact of the Allee effect parameter a_1 on the system's behavior, we vary a_1 from 0.5 to 2.025. The system exhibits an unstable limit cycle around E_3, as shown in Figure 5(c),(d). Figure 6(a)–(c) depicts the different steady-state behaviours of each population in the system (3.2) as a_1 varies. At $a_1 = 2.025$, a Hopf point (H) and a limit point (LP) coincide, with the first Lyapunov coefficient being 0.0059. This positive coefficient indicates that an unstable limit cycle bifurcates from H, leading to the loss of stability in the system (3.2). A branch point (BP) at $a_1 = 1.40$ exhibits transcritical bifurcations.

When b_1 is treated as a free parameter, the system exhibits three branch points at 0.10, 0.84, and 0. Additionally, one H and one LP coincide at $b_1 = 1.33$ with a first Lyapunov coefficient of 0.0029 (cf. Figure 7(a)–(c)). We also consider c_1 as the free parameter for the proposed system. We simulate a BP at 0.218, and one H and one LP at 0.186 (cf. Figure 8(a)–(c)). To illustrate the different steady-state behaviours of each population, we plot various values of $\hat{d}_1$ in Figure 9(a)–(c). At $\hat{d}_1 = 0.183$, a Hopf point and three transcritical bifurcations occur at $\hat{d}_1 = 0.20,\ 0.50$, and 0.029, denoted by the symbol BP.

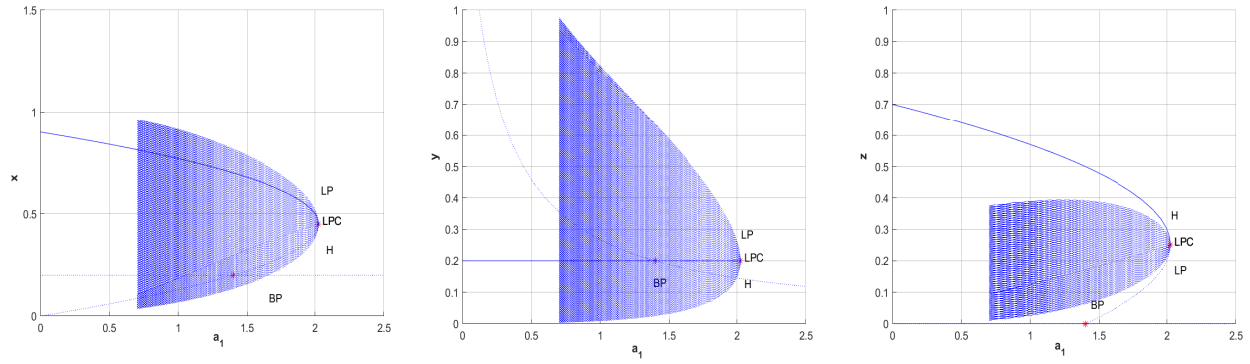

(a) (b) (c)

Figure 6. (a)–(c) The trajectory represents the different dynamic behaviors of each species for a_1.

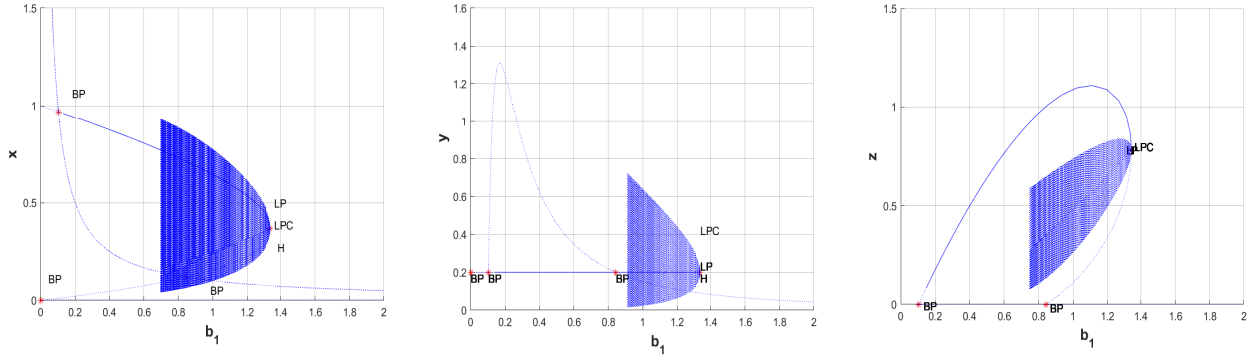

(a) (b) (c)

Figure 7. (a)–(c) The trajectory represents the different dynamic behaviors of each species for b_1.

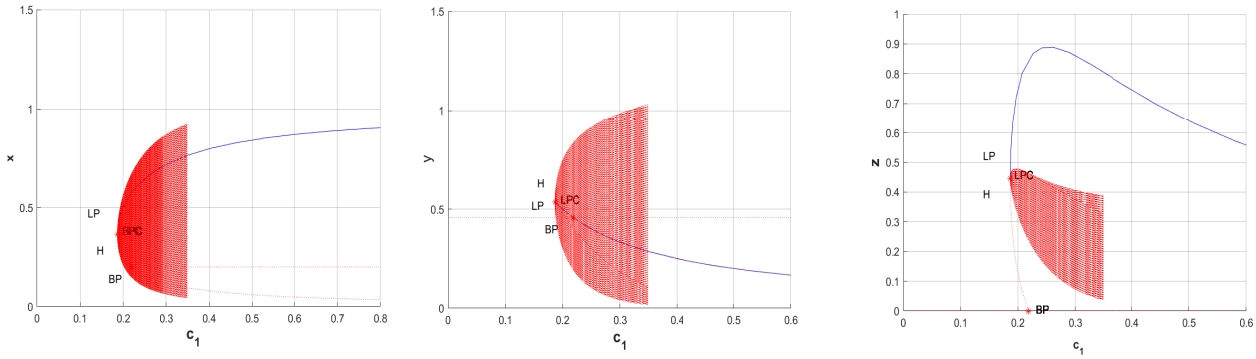

(a) (b) (c)

Figure 8. (a)–(c) The trajectory represents the different dynamic behaviors of each species for c_1.

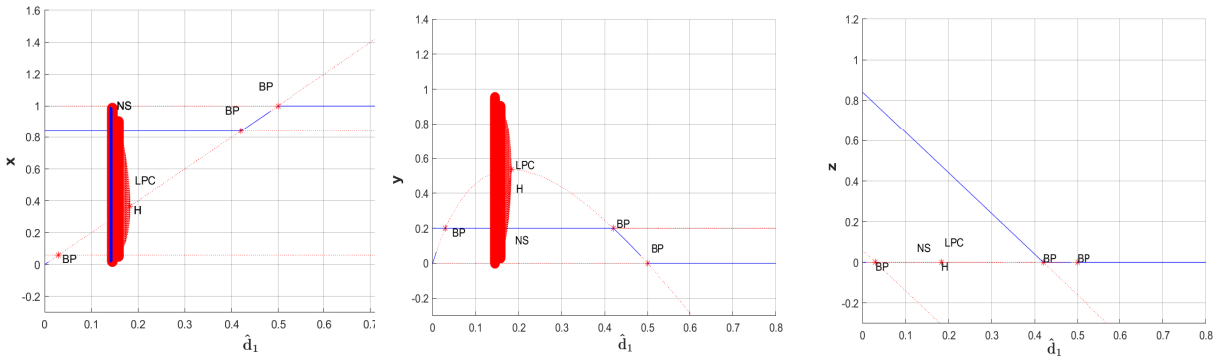

(a) (b) (c)

Figure 9. (a)–(c) The trajectory represents the different dynamic behaviors of each species for d_1.

6.2. Allee effect with fear

In this section, utilizing a numerical approach, we examine the dynamic characteristics of a three-trophic food chain system with the Allee effect and fear. We begin the analysis with the following parametric values:

$$a_1 = 0.5,\ b_1 = 0.5,\ c_1 = 0.5,\ \hat{d}_1 = 0.1,\ \hat{d}_2 = 0.1, \hat{f} = 0.2. \tag{6.1}$$

We observe that the coexistence and stability conditions for each species are satisfied. The coexistence equilibrium point, $\hat{E}_3 = (0.83, 0.20, 0.63)$, is locally asymptotically stable as a stable focus (see Figure 10(a),(b)). Next, we vary several sensitive parameters to demonstrate different system behaviors.

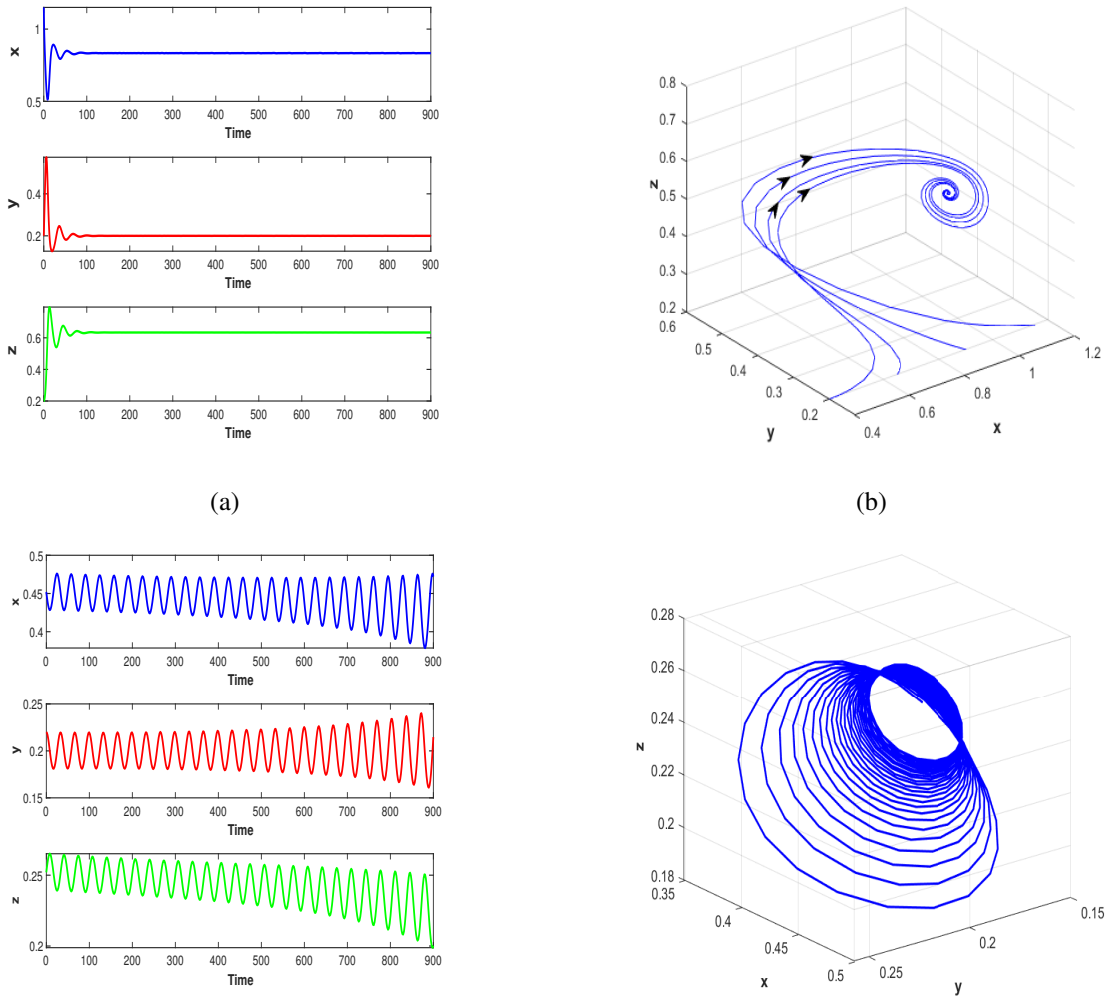

Figure 10. Panels (a) and (b) show, respectively, the time-series of the three species and the phase-plane portrait around the coexistence equilibrium $\hat{E}_3$ for $a_1 = 0.5$, $b_1 = 0.5$, $c_1 = 0.5$, $\hat{d}_1 = 0.1$, $\hat{d}_2 = 0.1$, and $\hat{f} = 0.2$ with the initial condition $[x(0), y(0), z(0)] = [0.452, 0.22, 0.252]$. Panels (c) and (d) display the analogous time-series and phase portrait when a Hopf bifurcation occurs at $\hat{E}_3$, with the same parameter values except $a_1 = 2.025$ (all other parameters and the initial condition unchanged).

6.2.1. Effects of a_1

By keeping all parameters constant except for a_1, the system (3.2) exhibits unstable behavior around the coexistence equilibrium $\hat{E}_3$ as a_1 increases from 0.5 to 2.025 (Figure 10(c),(d)). Figure 11(a)–(c) show the steady-state behaviour of each population for varying a_1 values. At $a_1 = 1.92$, a Hopf point (H) and a limit point (LP) coincide, denoted by red stars. Additionally, a branch point (BP) is located at $a_1 = 1.33$. The first Lyapunov coefficient for the Hopf point is 5.946802×10^3, indicating an unstable limit cycle. The symbol BP denotes a transcritical bifurcation at the branch point.

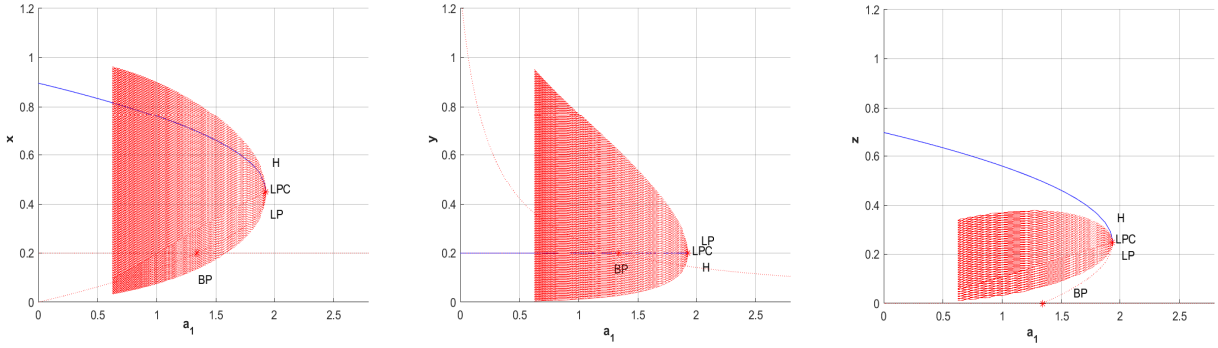

(a) (b) (c)

Figure 11. (a)–(c) The trajectory represents the different dynamic behaviors of each species respectively for a_1.

6.2.2. Effects of b_1

Keeping all parameters constant except for b_1, the system (3.2) demonstrates different steady-state behaviors (cf. Figure 12(a)–(c)). At $b_1 = 1.33$, one H and one LP coincide, which is denoted by red stars. Three BPs are at 0.844, 0.103, and 0. The first Lyapunov coefficient for the H is 2.986304×10^4, indicating an unstable limit cycle.

6.2.3. Effects of c_1

By varying c_1 while keeping all the other parameters constant, the system (3.2) shows different steady-state behaviours, as depicted in Figure 13(a)–(c). At $c_1 = 0.186$, one H and one LP coincide, marked by red stars. Additionally, a BP is located at 0.218. The first Lyapunov coefficient for the H is -2.446143×10^6, indicating a stable limit cycle.

6.2.4. Effects of $\hat{d}_1$

By varying $\hat{d}_1$ while keeping the other parameters constant, the system (3.2) exhibits different steady-state behaviors (see Figure 14(a)–(c)). At $\hat{d}_1 = 0.183$, one H appears with a first Lyapunov coefficient of -0.173, indicating a stable limit cycle. Additionally, three BPs are found at 0.416, 0.50, and 0.03, with the BPs denoting transcritical bifurcations.

6.2.5. Effects of $\hat{f}$

By varying $\hat{f}$ while keeping the other parameters constant, the system (3.2) exhibits different steady-state behaviors (see Figure 15(a)–(c)). At $\hat{f} = 8.39$, one H and one LP coincide, marked by red stars. The first Lyapunov coefficient for the H is 4.543526×10^4, indicating an unstable limit cycle. The BP located at 6.42 represents a transcritical bifurcation.

6.3. Two-parameter bifurcation

Various dynamic regimes are illustrated in the bifurcation diagrams for the parameters $a_1 - b_1$, $a_1 - \hat{f}$, $b_1 - \hat{f}$, $c_1 - \hat{f}$, as shown in Figure 16(a)–(d). Additionally, Tables 3 and 4 summarizes the findings for

the system (3.2), detailing the equilibrium point characteristics in the predator-prey interaction model.

Table 3. Characteristics of equilibrium points for the system (3.2) without fear.

Parameters	Values	Eigenvalues	Equilibrium points
a_1	2.025	$(0, \pm 0.187i)$	Hopf (H)
	2.025	$(0, \pm 0.187i)$	Limit point (LP)
	1.40	$(0, 0.031 \pm 0.094i)$	Branch point (BP)
b_1	1.33	$(0, \pm 0.412i)$	Hopf (H)
	1.33	$(0, \pm 0.412i)$	Limit point (LP)
	0.103	$(0, -0.003, -0.628)$	Branch point (BP)
	0.844	$(0, 0.056 \pm 0.116i)$	Branch point (BP)
	0.0	$(0, 1, -1)$	Branch point (BP)
c_1	0.186	$(0, \pm 0.239i)$	Hopf (H)
	1.86	$(0, \pm 0.239i)$	Limit point (LP)
	0.218	$(0, 0.053 \pm 0.141i)$	Branch point (BP)
$\hat{d_1}$	0.183	$(0.167, \pm .221i)$	Hopf (H)
	0.420	$(0, -0.11, -0.37)$	Branch point (BP)
	0.50	$(0, -0.10, -0.66)$	Branch point (BP)
	0.029	$(0, 0.041 \pm 0.035i)$	Branch point (BP)

Table 4. Characteristics of equilibrium points for the system (3.2) with fear

Parameters	Values	Eigenvalues	Equilibrium points
a_1	1.92	$(0, \pm 0.188i)$	Hopf (H)
	1.92	$(0, \pm 0.188i)$	Limit point (LP)
	1.33	$(0, 0.031 \pm 0.097i)$	Branch point (BP)
b_1	1.28	$(0, \pm 0.404i)$	Hopf (H)
	1.28	$(0, \pm 0.404i)$	Limit point (LP)
	0.103	$(0, -0.003, -0.60)$	Branch point (BP)
	0.824	$(0, 0.054 \pm 0.118i)$	Branch Point (BP)
	0.0	$(0, 1, -1)$	Branch point (BP)
c_1	0.204	$(0, \pm 0.238i)$	Hopf (H)
	0.204	$(0, \pm 0.238i)$	Limit point (LP)
	0.237	$(0, 0.048 \pm 0.142i)$	Branch point (BP)
$\hat{d_1}$	0.183	$(0.144, \pm .220i)$	Hopf (H)
	0.417	$(0, -0.129, -0.333)$	Branch point (BP)
	0.50	$(0, -0.10, -0.66)$	Branch point (BP)
	0.031	$(0, 0.041 \pm 0.039i)$	Branch point (BP)
$\hat{f_1}$	8.39	$(0, \pm .195i)$	Hopf (H)
	8.39	$(0, \pm .195i)$	Branch point (BP)
	6.42	$(0, 0.023 \pm 0.122i)$	Branch point (BP)
	0.031	$(0, 0.041 \pm 0.039i)$	Branch point (BP)

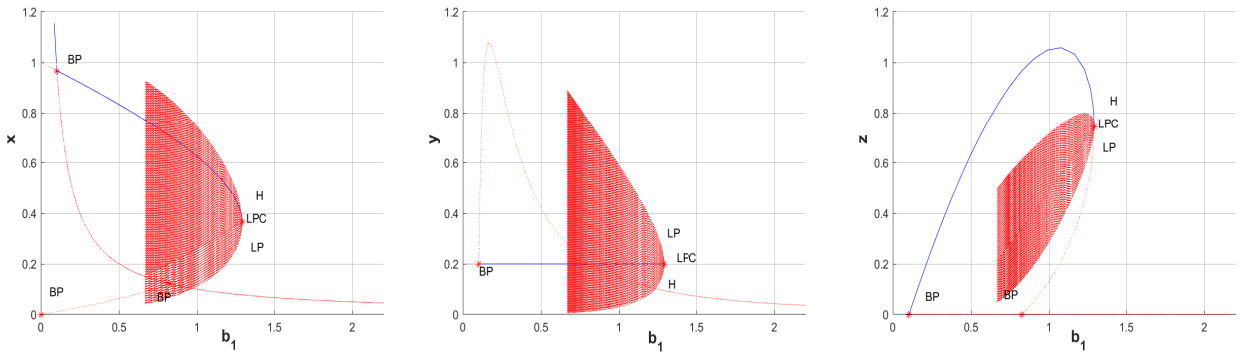

(a) (b) (c)

Figure 12. (a)–(c) The trajectory represents the different dynamic behaviors of each species respectively for b_1.

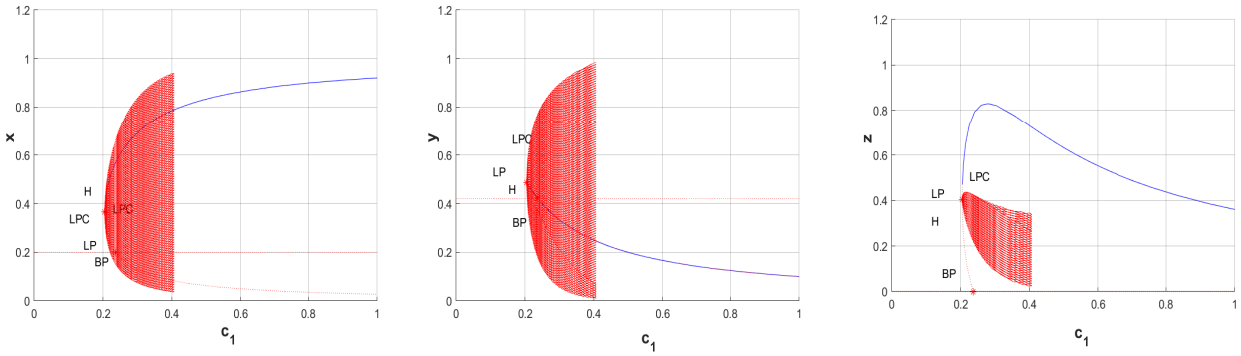

(a) (b) (c)

Figure 13. (a)–(c) The trajectory represents the different dynamic behaviors of each species respectively for c_1.

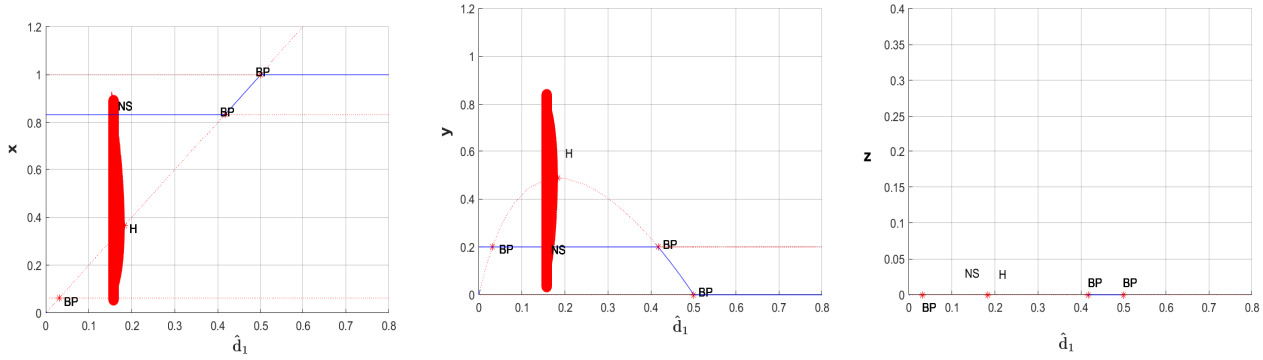

(a) (b) (c)

Figure 14. (a)–(c) The trajectory represents the different dynamic behaviors of each species for $\hat{d}_1$.

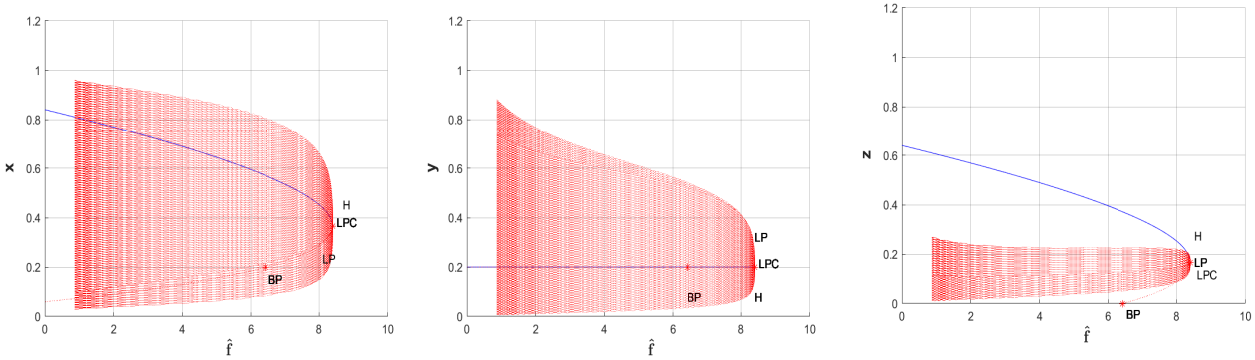

(a) (b) (c)

Figure 15. (a)–(c) The trajectory represents the different dynamic behaviors of each species for $\hat{f}$.

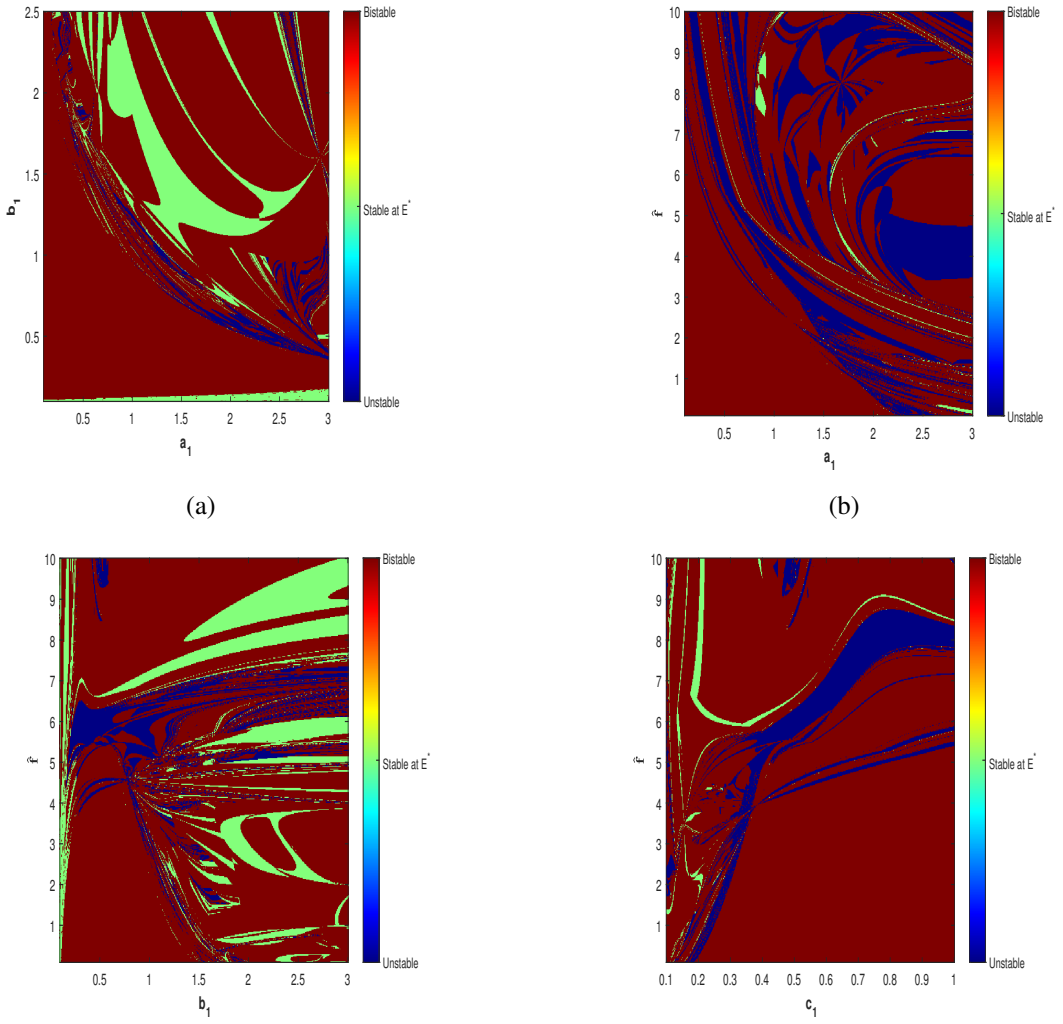

Figure 16. (a)–(d) Two-parameter bifurcation diagram for $a_1 - b_1$, $a_1 - \hat{f}$, $b_1 - \hat{f}$, and $c_1 - \hat{f}$, respectively.

6.4. Global sensitivity analysis

A mathematical technique called global sensitivity analysis (GSA) is used to measure how much each input parameter contributes to the overall variability of a model's output. GSA examines the impact of parameters while accounting for their whole range of likely values, in contrast to local sensitivity approaches that evaluate impact close to a fixed point [44]. The partial rank correlation coefficient (PRCC) is a popular GSA technique because of its ability to handle monotonic yet nonlinear correlations between inputs and outputs. Using rank-transformed data to reduce nonlinearity, the PRCC calculates the correlation between each input parameter and model output after eliminating the linear effects of all other parameters. Because of this, the PRCC is an effective tool for comprehending models' behavior and setting priorities for parameters for additional research, uncertainty assessment, or experimental design.

Sensitivity is depicted in a bar graph, where the bar length represents the degree of sensitivity.

A parameter is deemed sensitive if its PRCC value exceeds ± 0.5. As shown in Figure 17, most parameters in the system (3.2) are sensitive.

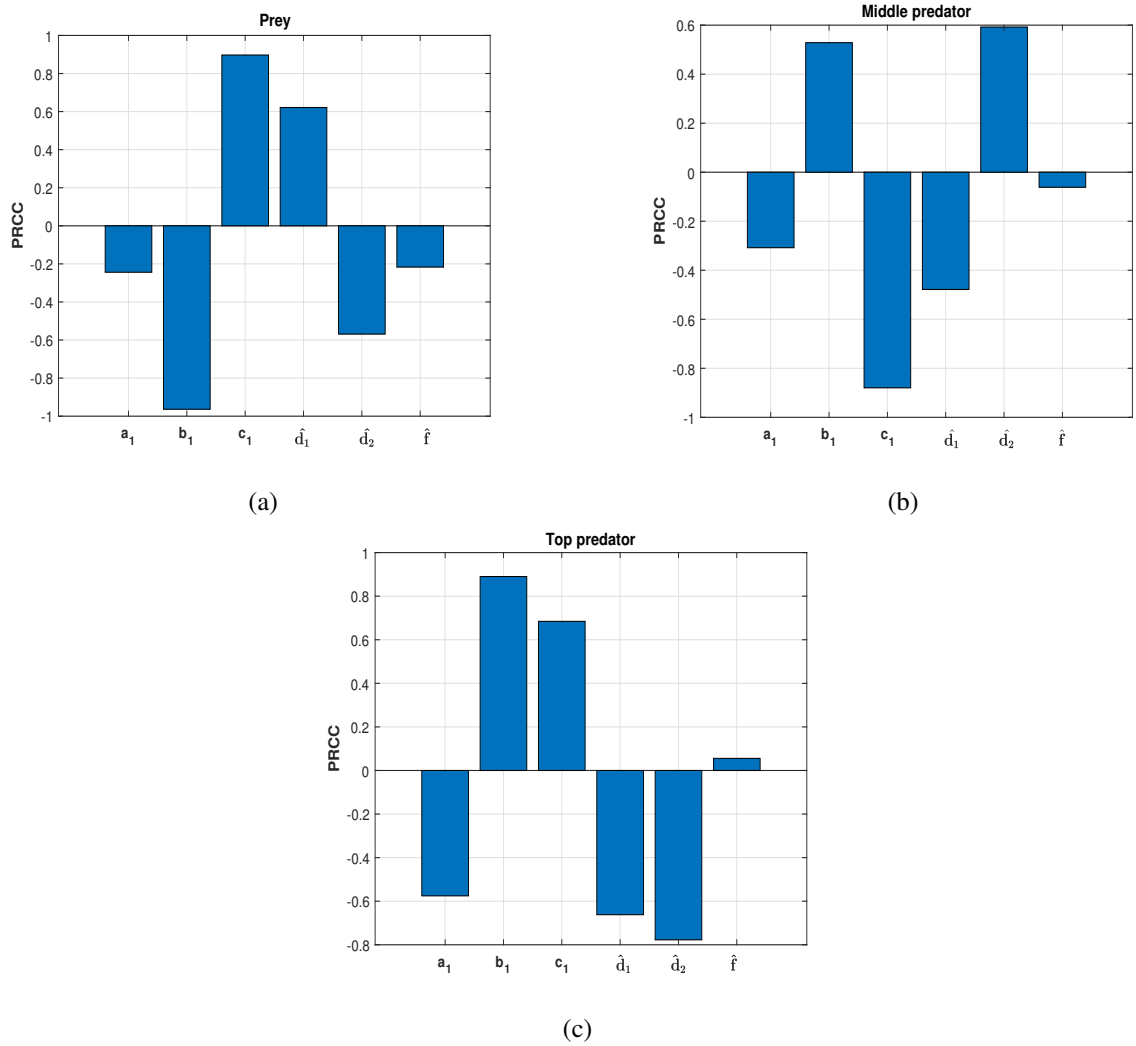

(a) (b)

(c)

Figure 17. Sensitivity analysis depicting estimated parameters for prey, predator, and super-predator populations, respectively.

6.5. The spatio-temporal model and patterns

In this subsection, we present the numerical simulations of the system (5.3) for a better understanding of the spatiotemporal dynamics and pattern formation. The temporal part of the model system (5.3) is solved using Euler's explicit method, and a five-point stencil finite difference scheme is used for the diffusion part. All the numerical simulations employ the zero-flux boundary conditions on the domain of size 100×100. The space and time steps are taken as $\Delta h = 0.5$ and $\Delta t = 0.01$. In every pattern, the blue colour corresponds to the low species density, and the orange colour corresponds to the moderately high species density. The initial species distribution is small random perturbations about the homogeneous steady state E^*. We simulate a large value of t to explore the stationary patterns.

In Example 1, we show that the cross-diffusion induced Turing instability, which occurs in the system (5.3) for the given set of parameters (5.13). At $d_{12} = 0.4$ and the remaining parameters are the same as given in Example 1, labyrinthine– type patterns are observed for the prey, predator, and top predator species (cf. Figure 18). Figure 18 shows that patches of high prey density alternate with patches of high predator density. This patchiness allows prey populations to persist in certain areas while predators are sustained in others, reducing the risk of local extinctions. Moreover, high-density regions of prey correspond to low-density regions of the predator. Thus, both prey and predator are negatively correlated.

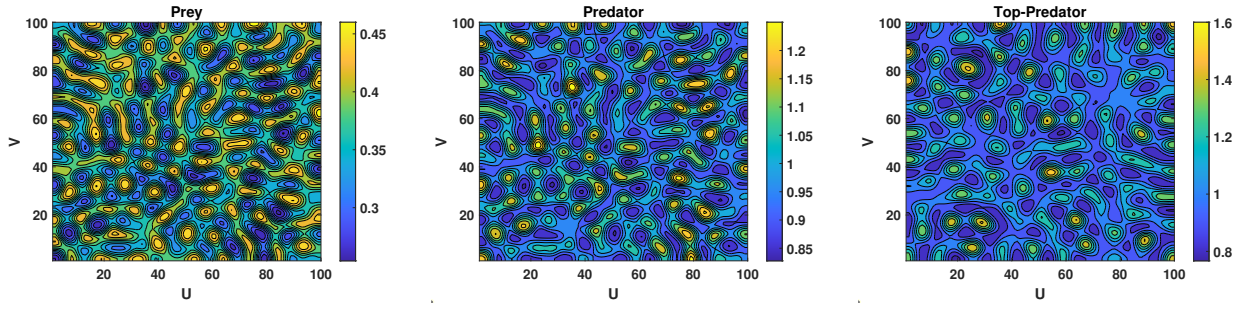

(a) (b) (c)

Figure 18. Snapshots of Turing patterns for the parameters (5.13) with $d_{12} = 0.4$ at 500 days.

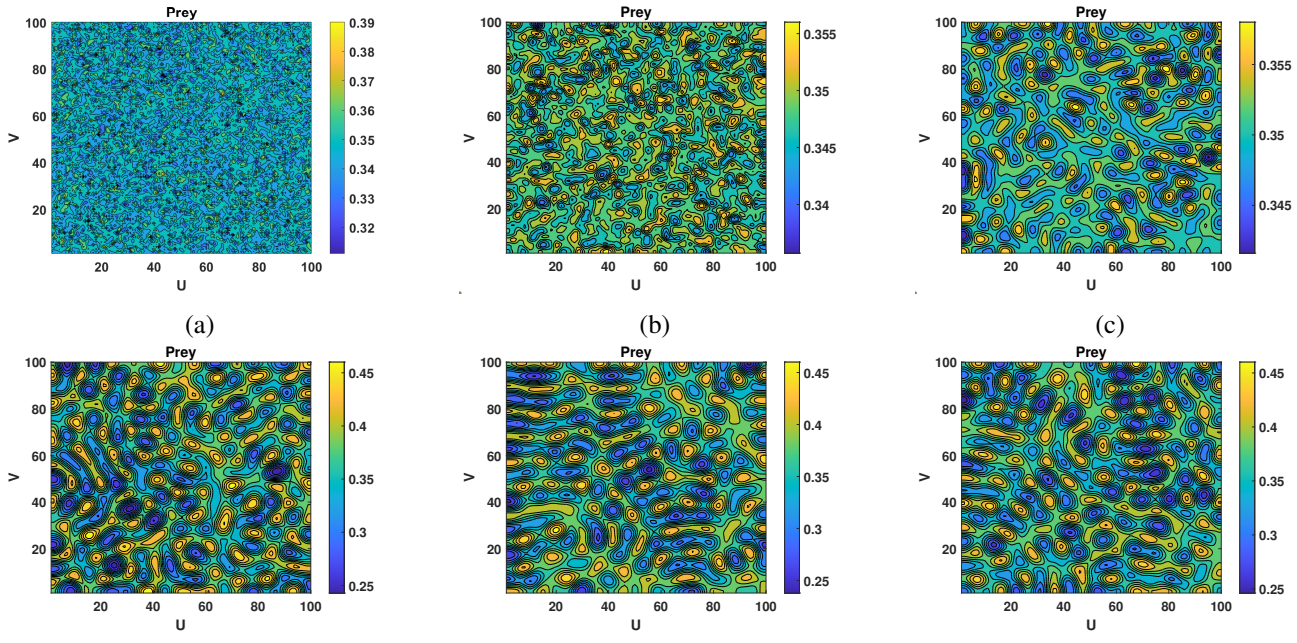

(a) (b) (c)

(d) (e) (f)

Figure 19. Snapshots of contour pictures of the time evaluation of prey species at (a) $t = 0$, (b) 10, (c) 100, (d) 500, (e) 1000 (f) 1500 days for the parameters (5.13) with $d_{12} = 0.4$.

In Figure 19, we present the evolution process of labyrinthine– type patterns shown in the Figure 18 taking time $t = 0,\ 10,\ 100,\ 500,$ and 1000 days. In particular, we present the Turing patterns for the prey population. At $t = 0$ and $t = 10$ days, the pattern structure is not clear (cf. Figure 19(a),(b)).

The labyrinthine-type patterns are observed (cf. Figure 19(c),(d)) for $t = 500$ days. When increasing the time further to 1000 days and 1500 days, patterns remain unaltered (cf. Figure 19(e),(f)), this indicates that the patterns are stationary patterns.

Next, in Figure 20, we show how the cross-diffusion of prey due to predators d_{12} impacts the occurrence of Turing patterns and their type. We have taken the same parameter values as given in (5.13) except d_{12}. Initially, at $d_{12} = 0.04$, the high density of the prey population is located in the form of a small circular patch, and the remaining domain comprises a low density of prey (cf. Figure 20(a)). Increasing the value of $d_{12} = 0.06$, a high-density of prey population spreads over the entire domain (cf. Figure 20(b)). Biologically, as cross-diffusion of prey species increases, they disperse over the domain to avoid predation. When further increasing the value of $d_{12} = 0.1$ and $d_{12} = 0.3$, the prey population is distributed in the form of high-density and low-density patches (cf. Figure 20(c),(d)) and when further increasing the value of $d_{12} = 0.4$, the prey species spreads in the form of a labyrinthine–type pattern to ensure stable existence and to avoid the local extinction (cf. Figure 20(e)).

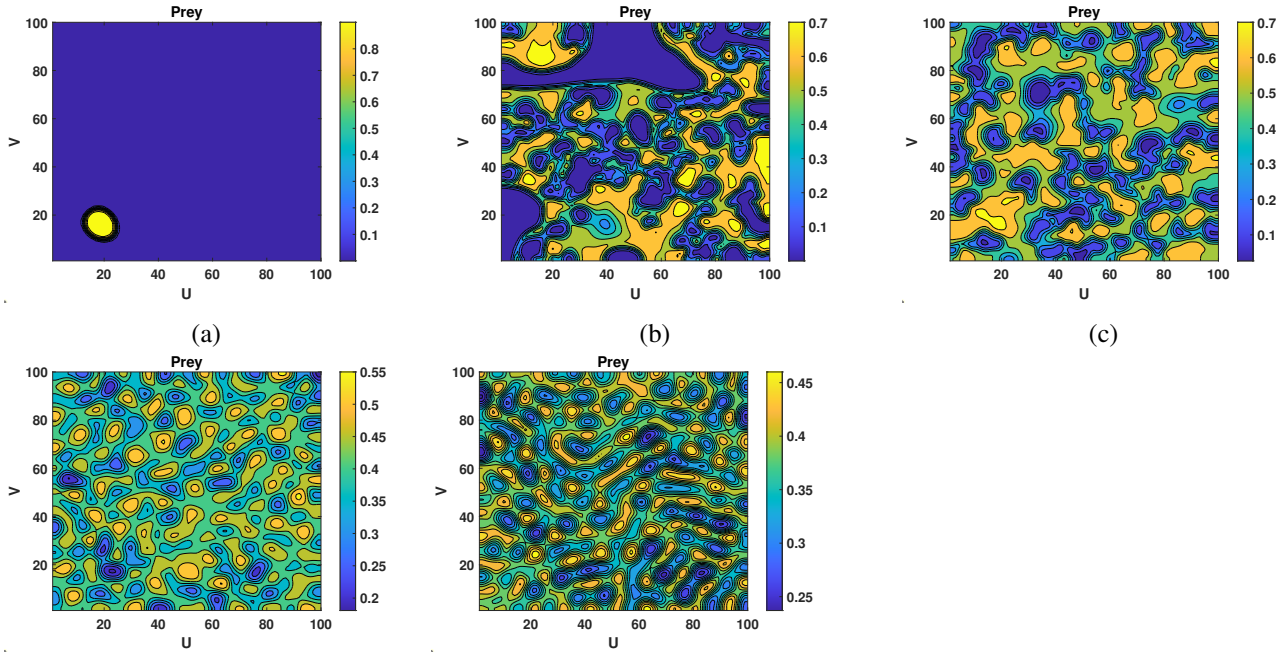

Figure 20. Snapshots of Turing patterns of prey species for different values of d_{12} at 500 days: (a) $d_{12} = 0.04$, (b) $d_{12} = 0.06$, (c) $d_{12} = 0.1$, (d) $d_{12} = 0.3$, (e) $d_{12} = 0.4$ for the parameters (5.13) with $d_{12} = 0.4$.

7. Conclusions and further work

In this paper, we show that the tri-trophic system remains bounded and is conditionally stable around four distinct equilibria (see "Stability Analysis"). Boundedness ensures that the population levels stay within realistic limits. We also demonstrate that the Allee effect has a profound influence on the system's dynamics, with the capacity to suppress chaotic fluctuations. Our analytical results reveal that varying the Allee parameter alters the local asymptotic stability at equilibrium E_2 and can trigger Hopf

bifurcations at both E_2 and E_3. By adjusting this parameter, one can therefore modulate the system's susceptibility to bifurcation and chaos, either amplifying or damping irregular dynamics. This finding positions the Allee effect as a practical biological control tool for maintaining ecological balance in prey-predator models.

We have also carried out detailed theoretical investigations and computer experiments, with the outcomes summarized in the "Numerical Simulations" section. In particular, we found the following.

- Taking b_1 as the bifurcation parameter and varying it over a chosen interval causes the system to exhibit a transcritical bifurcation at E_1, a Hopf bifurcation at E_2, or a saddle-node bifurcation at E_3.
- When only c_1 is varied, the model undergoes a transcritical bifurcation around E_2 and a saddle-node bifurcation at E_3 for certain parameter values.
- Treating $\hat{d}_1$ as the bifurcation parameter affects only E_1, which then undergoes a transcritical bifurcation.
- Finally, by choosing $\hat{d}_2$ as the bifurcation parameter (with all others held fixed), E_2 experiences a transcritical bifurcation and E_3 has a saddle-node bifurcation.

The predator-prey trajectories for each parameter sweep are displayed in the "Numerical Simulations" section, and the bifurcation boundaries—i.e., the critical intersection points—have been identified through numerical computation.

To incorporate the fear effect, we modify the prey dynamics, yielding the system (3.2). Our results show that each parameter profoundly influences the population's behavior, and that both the fear effect and the Allee effect are essential for stabilizing the system (3.2).

We also extended the purely temporal system (3.2) into a spatiotemporal one by adding both self-diffusion and density-dependent cross-diffusion terms. We then examined how these diffusion coefficients affect the coexistence that was found in the non-spatial model. In particular, the prey's cross-diffusion in response to predators, d_{12}, plays a pivotal role in the emergence of spatial patterns. Once diffusion is introduced, the previously stable, spatially homogeneous steady state of the model (5.3) loses its stability and gives rise to labyrinthine structures. For example, with $d_{12} = 0.4$ (while all other parameters remain as in Eq (5.13), the prey, predator, and top–predator densities organize themselves into intertwined, maze-like patterns.

This cross-diffusion coefficient not only generates these patterns but also regulates the spatial dynamics overall. Through the cross-diffusion terms, prey and predators develop a strong negative correlation: areas with high prey density exhibit lower predator density, reflecting the prey's group defense strategy. Such spatial segregation allows the prey to persist in protected refuges while predators occupy adjacent zones, thereby lowering the risk of local extinction.

Finally, we found that increasing the parameter $a_1 = \frac{n}{k}$, which represents the Allee effect threshold, has a destabilizing influence on the spatial dynamics of the system (5.3).

The summary highlights how leaser slime patterns describe the remarkable behaviors and ecological functions of slime molds. Evolving from bacteria, these organisms exhibit exceptional adaptability and resource optimization, often compared to network-optimization processes in advanced systems. Recent research examines food chain dynamics incorporating fear and Allee effects, revealing emergent leaser slime patterns. Ecologically, slime moulds are pivotal in nutrient cycling and soil health, as they decompose organic matter and facilitate decomposition. Their distinctive movement and growth

strategies not only shed light on fundamental biological processes but also inspire computational and network design algorithms. By occupying a transitional position between simple microorganisms and more complex life forms (such as fungi, plants, and animals), slime molds challenge conventional species boundaries and underscore the continuum of life's organizational complexity.

Nutrient cycling: slime molds, such as those exhibiting leaser slime patterns, play a significant role in the decomposition of organic matter. They help break down dead plant material, release nutrients into the soil, support plant growth, and maintain soil health. This process is vital for ecosystems' nutrient cycling [40]. The current study explores how Leaser Slime patterns can appear for the case of fear and Allee effects.

Microbial interactions: leaser slime patterns can be a model for studying microbial interactions. These organisms often interact with bacteria and other microorganisms, influencing community dynamics and competition. Understanding these interactions can provide insights into microbial ecology and the functioning of microbial communities [41]. The current study sheds light on the issue of microbial community and provides a qualitative and quantitative analysis of the parameters for which leaser slime patterns can be observed.

Biodiversity indicators: Slime molds—and especially those exhibiting distinctive "leaser slime" patterns—serve as sensitive gauges of ecosystems' health and overall biodiversity. Because their populations respond quickly to environmental fluctuations, shifts in slime molds' abundance can act as early warnings of habitat change or degradation (see [36]).

Finally, our work departs from—and extends—previous models in several important ways.
(1) Joint Allee and fear effects

- Previous studies typically treat the Allee effect or the fear effect in isolation.
- We integrate both phenomena simultaneously in a tri-trophic food-chain framework, capturing a richer set of predator-prey dynamics.

(2) In-depth bifurcation analysis

- We perform a full suite of bifurcation analyses (transcritical, Hopf, and saddle-node) at each equilibrium.
- This reveals ecological thresholds and transition behaviors that prior research has overlooked.

(3) Rigorous numerical and analytical validation

- Extensive simulations corroborate our theoretical findings.
- We uncover complex spatiotemporal behaviours—including chaotic regimes—that underscore the model's realism.

(4) Spatial model with cross-diffusion

- By embedding cross-diffusion terms into a reaction–diffusion system, we explore biologically meaningful pattern formation.
- This extension produces "leaser slime"–like spatial structures, a novel outcome in the context of tri-trophic interactions.

(5) Global sensitivity and Turing instability

- We introduce a global sensitivity analysis using PRCCs.

- Our model also exhibits Turing instabilities, offering fresh insights into pattern emergence.

Table 5. Comparison of the proposed model with existing ecological models (e.g., [16, 17, 45–48]).

Feature	Classical Models [16, 17, 45]	Allee-only Models [46, 48]	Proposed Model
Ecological Structure	Prey–predator or Tri-trophic food chain	Tri-trophic models with Allee effect	Tri-trophic model with Allee and fear effects
Allee effect	Not considered	Considered (mostly in prey)	Considered with spatial extension
Fear effect	Not included	Not included	Explicitly incorporated as functional modifier of prey growth in a two-species model [47]
Spatial dynamics	ODE models only	ODE or basic PDE models	PDE system with cross-diffusion (spatial effects and pattern formation)
Bifurcation analysis	Limited (typically Hopf only)	Hopf/transcritical in some cases	Multiple bifurcations: Hopf, transcritical, and saddle-node with parameter thresholds
Sensitivity analysis	Often absent or qualitative	Rarely included	Quantitative PRCC-based global sensitivity analysis
Pattern formation	Not addressed	Rarely studied	Emergence of Turing-type patterns and "leaser slime" morphology
Mathematical novelty	Classical stability or numerical only	Limited to Allee impact on equilibria	Comprehensive analysis including spatial stability, cross-diffusion, and nonlinear sensitivity

Table 5 compares these features side by side with earlier approaches (e.g., [18, 31]). Unlike models that omit fear effects, cross-diffusion, or multi-parameter bifurcations, our framework unifies these elements to provide a more comprehensive and ecologically realistic portrayal of multi-species stability and pattern formation.

Use of AI tools declaration

The authors declare that they have not used Artificial Intelligence (AI) tools in the creation of this article.

Acknowledgments

The authors thank the associate editor and the anonymous reviewers for valuable comments, which contributed to the improvement in the presentation of the paper.

Conflict of interest

The authors declare there is no conflict of interest.

References

1. G. Q. Sun, H. T. Zhang, J. S. Wang, J. Li, Y. Wang, L. Li, et al, Mathematical modeling and mechanisms of pattern formation in ecological systems: A review, *Nonlinear Dyn.*, **104** (2021), 1677–1696. https://doi.org/10.1007/s11071-021-06314-5
2. D. O'Sullivan, G. L. Perry, *Spatial Simulation: Exploring Pattern and Process*, John Wiley & Sons, 2023.

3. J. T. Tanner, The stability and the intrinsic growth rates of prey and predator populations, *Ecology*, **56** (1975), 855–867. https://doi.org/10.2307/1936296
4. O. D. Feo, S. Rinaldi, Yield and dynamics of tritrophic food chains, *Am. Nat.*, **150** (1997), 328–345. https://doi.org/10.1086/286068
5. S. Gakkhar, R. K. Naji, Order and chaos in predator to prey ratio-dependent food chain, *Chaos Solitons Fractals*, **18** (2003), 229–239. https://doi.org/10.1016/S0960-0779(02)00642-2
6. S. B. Hsu, T. W. Hwang, Y. Kuang, A ratio-dependent food chain model and its applications to biological control, *Math. Biosci.*, **181** (2003), 55–83. https://doi.org/10.1016/S0025-5564(02)00127-X
7. S. Pathak, A. Maiti, G. P. Samanta. Rich dynamics of a food chain model with Hassell-Varley type functional responses, *Appl. Math. Comput.* **208** (2009), 303–317.https://doi.org/10.1016/j.amc.2008.12.015
8. R. K. Upadhyay, R. K. Naji, Dynamics of a three species food chain model with Crowley-Martin type functional response, *Chaos Solitons Fractals*, **42** (2009), 1337–1346. https://doi.org/10.1016/j.chaos.2009.03.020
9. M. Haque, N. Ali, S. Chakravarty, Study of a tri-trophic prey-dependent food chain model of interacting populations, *Math. Biosci.*, **246** (2013), 55–71. https://doi.org/10.1016/j.mbs.2013.07.021
10. D. Pattanayak, A. Mishra, S. K. Dana, N. Bairagi, Bistability in a tri-trophic food chain model: Basin stability perspective, *Chaos*, **31** (2021), 073124. https://doi.org/10.1063/5.0054347
11. W. Feng, N. Rocco, M. Freeze, X. Lu, Mathematical analysis on an extended Rosenzweig-MacArthur model of tri-trophic food chain, *Discrete Contin. Dyn. Syst. S*, **7** (2014), 1215–1230. https://doi.org/10.3934/dcdss.2014.7.1215
12. Y. A. Kuznetsov, O. De Feo, S. Rinaldi, Belyakov homoclinic bifurcations in a tritrophic food chain model, *SIAM J. Appl. Math.*, **62** (2001), 462–487. https://doi.org/10.1137/S0036139900378542
13. S. Lv, M. Zhao, The dynamic complexity of a three species food chain model, *Chaos Solitons Fractals*, **37** (2008), 1469–1480. https://doi.org/10.1016/j.chaos.2006.10.057
14. B. W. Kooi, L. D. J Kuijper, M. P. Boer, S. A. L. M. Kooijman, Numerical bifurcation analysis of a tri-trophic food web with omnivory, *Math. Biosci.*, **177** (2002), 201–228. https://doi.org/10.1016/S0025-5564(01)00111-0
15. Y. Chen, J. Yu, C. Sun, Stability and Hopf bifurcation analysis in a three-level food chain system with delay, *Chaos Solitons Fractals*, **31** (2007), 683–694. https://doi.org/10.1016/j.chaos.2005.10.020
16. J. G. Wang, X. Y. Meng, L. Lv, J. Li, Stability and bifurcation analysis of a Beddington-DeAngelis prey-predator model with fear effect, prey refuge and harvesting, *Int. J. Bifurc. Chaos*, **33** (2023), 2350013. https://doi.org/10.1142/S021812742350013X
17. Z. Liang, X. Meng, Stability and Hopf bifurcation of a multiple delayed predator-prey system with fear effect, prey refuge and Crowley–Martin function, *Chaos Solitons Fractals*, **175** (2023), 113955. https://doi.org/10.1016/j.chaos.2023.113955

18. J. C. Gascoigne, R. N. Lipcius, Allee effects driven by predation, *J. Appl. Ecol.*, **41** (2004), 801–810. https://doi.org/10.1111/j.0021-8901.2004.00944.x
19. J. M. Drake, A. M. Kramer, Allee effects, *Nat. Educ. Knowl.*, **3** (2011), 2.
20. E. A. Coddington, N. Levinson, *Theory of Ordinary Differential Equations*, McGraw-Hill, New York, 1955.
21. P. Hartman, *Theory of Ordinary Differential Equations*, Society for Industrial and Applied Mathematics, 2002.
22. L. Perko, *Differential Equations and Dynamical Systems*, Springer Science & Business Media, 2013
23. A. Pazy, *Semigroups of Linear Operators and Applications to Partial Differential Equations*, Springer Science & Business Media, 2012
24. D. Henry, *Geometric Theory of Semilinear Parabolic Equations*, Springer, 2006.
25. L. C. Evans, *Partial Differential*, American Mathematical Society, RI, USA, 2010.
26. J. Smoller, *Shock Waves and Reaction-Diffusion Equations*, Springer Science & Business Media, 2012.
27. J. D. Murray, *Mathematical Biology II: Spatial Models and Biomedical Applications*, Springer New York, 2003. https://doi.org/10.1007/b98869
28. M. C. Cross, P. C. Hohenberg, Pattern formation outside of equilibrium, *Rev. Mod. Phys.*, **65** (1993), 851. https://doi.org/10.1103/RevModPhys.65.851
29. V. I. Arnold, *Ordinary Differential Equations*, Springer Science & Business Media, 1992.
30. B. Xie, Impact of the fear and Allee effect on a Holling type II prey-predator model, *Adv. Differ. Equations*, **2021** (2021), 464. https://doi.org/10.1186/s13662-021-03592-6
31. X. Wang, L. Zanette, X. Zou, Modelling the fear effect in predator-prey interactions, *J. Math. Biol.*, **73** (2016), 1179–1204. https://doi.org/10.1007/s00285-016-0989-1
32. M. Haque, M. S. Rahman, E. Venturino, B. L. Li, Effect of a functional response-dependent prey refuge in a predator-prey model, *Ecol. Complex.*, **20** (2014), 248–256. https://doi.org/10.1016/j.ecocom.2014.04.001
33. M. S. Rahman, S. Pramanik, E. Venturino, An ecoepidemic model with healthy prey herding and infected prey drifting away, *Nonlinear Anal.*, **28** (2023), 326–364. https://doi.org/10.15388/namc.2023.28.31549
34. B. Mukhopadhyay, R. Bhattacharyya, A stage-structured food chain model with stage dependent predation: Existence of codimension one and codimension two bifurcations, *Nonlinear Anal. Real World Appl.*, **12** (2011), 3056–3072. https://doi.org/10.1016/j.nonrwa.2011.05.007
35. M. Haque, Existence of complex patterns in the Beddington-DeAngelis predator-prey model, *Math. Biosci.*, **239** (2012), 179–190. https://doi.org/10.1016/j.mbs.2012.05.006
36. L. N. Guin, M. Haque, P. K. Mandal, The spatial patterns through diffusion-driven instability in a predator-prey model, *Appl. Math. Modell.*, **36** (2012), 1825–1841. https://doi.org/10.1016/j.apm.2011.05.055

37. N. Shigesada, K. Kawasaki, E. Teramoto, Spatial segregation of interacting species, *J. Theor. Biol.*, **79** (1979), 83–99. https://doi.org/10.1016/0022-5193(79)90258-3

38. E. H. Kerner, A statistical mechanics of interacting biological species, *Bull. Math. Biophys.*, **19** (1957), 121–146. https://doi.org/10.1007/BF02477883

39. E. H. Kerner, Further considerations on the statistical mechanics of biological associations, *Bull. Math. Biophys.*, **21** (1959), 217–255. https://doi.org/10.1007/BF02476361

40. P. Schaap, Regulation of size and pattern in the cellular slime molds, *Differentiation*, **33** (1987), 1–16. https://doi.org/10.1111/j.1432-0436.1987.tb01535.x

41. J. T. Bonner, The pattern of differentiation in amoeboid slime molds, *Am. Nat.*, **86** (1952), 79–89. https://doi.org/10.1086/281707

42. S. L. Stephenson, J. C. Landolt, Dictyostelid cellular slime molds in canopy soils of tropical forests, *Biotropica*, **30** (1998), 657–661. https://doi.org/10.1111/j.1744-7429.1998.tb00105.x

43. A. Madzvamuse, H. S. Ndakwo, R. Barreira, Cross-diffusion-driven instability for reaction-diffusion systems: Analysis and simulations, *J. Math. Biol.*, **70** (2025), 709–743. https://doi.org/10.1007/s00285-014-0779-6

44. S. Marino, I. B. Hogue, C. J. Ray, D. E. Kirschner, A methodology for performing global uncertainty and sensitivity analysis in systems biology, *J. Theor. Biol.*, **254** (2008), 178–196. https://doi.org/10.1016/j.jtbi.2008.04.011

45. M. L. Rosenzweig, R. H. MacArthur, Graphical representation and stability conditions of predator-prey interactions, *Am. Nat.*, **97** (1963), 209–223. https://doi.org/10.1086/282272

46. F. Courchamp, T. Clutton-Brock, B. Grenfell, Inverse density dependence and the Allee effect, *Trends Ecol. Evol.*, **14** (1999), 405–410. https://doi.org/10.1016/S0169-5347(99)01683-3

47. S. K. Sasmal, Population dynamics with multiple allee effects induced by fear factors–A mathematical study on prey-predator interactions, *Appl. Math. Modell.*, **64** (2018), 1–14. https://doi.org/10.1016/j.apm.2018.07.021

48. S. Mandal, F. A. Basir, S. Ray, Additive Allee effect of top predator in a mathematical model of three species food chain, *Energy Ecol. Environ.*, **6** (2021), 451–461. https://doi.org/10.1007/s40974-020-00200-3

AIMS Press